(2)

AD No. _____

TECOM Project No. 8-CO-390-ASL-001

DPG No. DPG-FR-88-317

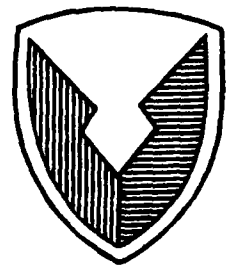

US ARMY
MATERIEL COMMAND

TEST REPORT

FIELD TEST OF

A CROSSWIND SCINTILLOMETER

BY

CHRISTOPHER A.BILTOFT

Meteorology Division
Materiel Test Directorate

U.S. ARMY DUGWAY PROVING GROUND
DUGWAY, UTAH 84022-5000

JULY 1988

Disposition Instructions

Destroy this report when no longer needed. Do not return it to the originator.

Disclaimer Statement

The views, opinions, and findings in this report are those of the author and should not be construed as an official Department of the Army position, unless so designated by other official documentation.

Trade Name Statement

The use of trade names in this report does not constitute an official endorsement or approval of the use of such commercial hardware or software. This report may not be cited for purposes of advertisement.

SECURITY CLASSIFICATION OF THIS PAGE

REPORT DOCUMENTATION PAGE

Form Approved OMB No. 0704-0188

1a. REPORT SECURITY CLASSIFICATION: UNCLASSIFIED	1b. RESTRICTIVE MARKINGS
2a. SECURITY CLASSIFICATION AUTHORITY	3. DISTRIBUTION / AVAILABILITY OF REPORT: Approved for Public Release; Distribution Unlimited
2b. DECLASSIFICATION / DOWNGRADING SCHEDULE	
4. PERFORMING ORGANIZATION REPORT NUMBER(S): DPG-FR-88-317	5. MONITORING ORGANIZATION REPORT NUMBER(S)
6a. NAME OF PERFORMING ORGANIZATION: U.S. Army Dugway Proving Ground; 6b. OFFICE SYMBOL (If applicable): STEDP MT-M	7a. NAME OF MONITORING ORGANIZATION
6c. ADDRESS (City, State, and ZIP Code): Dugway, Utah 84022-5000	7b. ADDRESS (City, State, and ZIP Code)
8a. NAME OF FUNDING / SPONSORING ORGANIZATION: LABCOM/U.S. Army Atmospheric Sciences Laboratory; 8b. OFFICE SYMBOL (If applicable): SLCAS AS-M	9. PROCUREMENT INSTRUMENT IDENTIFICATION NUMBER
8c. ADDRESS (City, State, and ZIP Code): White Sands, New Mexico 88002-5501	10. SOURCE OF FUNDING NUMBERS: PROGRAM ELEMENT NO. / PROJECT NO. 8-CO-390-ASL-001 / TASK NO. / WORK UNIT ACCESSION NO.

11. TITLE (Include Security Classification): FIELD TEST OF A CROSSWIND SCINTILLOMETER (UNCLASSIFIED)

12. PERSONAL AUTHOR(S): Biltoft, Christopher A.

13a. TYPE OF REPORT	13b. TIME COVERED	14. DATE OF REPORT (Year, Month, Day)	15. PAGE COUNT
Customer Report	FROM 87/11 TO 88/07	1988 July 21	

16. SUPPLEMENTARY NOTATION

17. COSATI CODES			18. SUBJECT TERMS (Continue on reverse if necessary and identify by block number)		
FIELD	GROUP	SUB-GROUP	aerovane	GMQ-11	spatial filtering
04	02		anemometer	path averaging	spatially-averaged filter
			crosswind	scintillometer	sonic anemometer

19. ABSTRACT (Continue on reverse if necessary and identify by block number)

Field tests of a prototype scintillometer that uses a spatially-averaged filter design for crosswind measurement were conducted at the Aberdeen Proving Ground Main Front Gun Range. The scintillometer measures wind components transverse to an optical path established between a transmitter and a receiver. The spatially-averaged filter design peaks wind measurement weighting functions at five segments along the optical path, producing simultaneous crosswind readings from these path segments. Scintillometer performance, evaluated using sonic anemometers, GMQ-11 aerovanes, and parallel scintillometer paths, is generally comparable to that of a high quality wind instrument. A performance problem was identified during cross-path wind reversals in light and variable winds, where ambiguities in the sign of the crossing wind component occasionally caused spurious wind readings. The scintillometer design is sufficiently robust for field use, and the transmitters and receivers are easy to set up, align, and operate. The crosswind scintillometer performed well in the field environment during exposure to adverse weather conditions, and appears to have significant test support applications.

20. DISTRIBUTION / AVAILABILITY OF ABSTRACT	21. ABSTRACT SECURITY CLASSIFICATION	
☒ UNCLASSIFIED/UNLIMITED ☐ SAME AS RPT. ☐ DTIC USERS	UNCLASSIFIED	
22a. NAME OF RESPONSIBLE INDIVIDUAL: Christopher A. Biltoft	22b. TELEPHONE (Include Area Code): (801) 831-5101	22c. OFFICE SYMBOL: STEDP MT-M

DD Form 1473, JUN 86 — Previous editions are obsolete. — SECURITY CLASSIFICATION OF THIS PAGE

UNCLASSIFIED

TABLE OF CONTENTS

ACKNOWLEDGMENTS

Field tests of the spatially-averaged filter scintillometer were performed by the Meteorology Division, Materiel Test Directorate, U.S. Army Dugway Proving Ground at the Aberdeen Proving Ground Main Front Gun Range. The author is indebted to Charles Clough and the Aberdeen Atmospheric Sciences Laboratory Meteorology Team for project support during the test series. The scintillometers were designed and built for Dugway Proving Ground by Gerard Ochs and James Wilson of the National Oceanic and Atmospheric Administration Environmental Research Laboratories/Wave Propagation Laboratory (NOAA ERL/WPL). Messers. Ochs and Wilson also assisted with instrument setup and operation for the test series. Sonic anemometer setup and data collection were performed by James Osterud of the Dugway Instrumentation Branch, and software development was provided by Gerald Wheeler of the Dugway Analytical Systems Branch. Mrs. Susan Gross provided the word processing support during report preparation. The field tests were funded by the U.S. Army Atmospheric Sciences Laboratory (SLCAS-AS-M), with technical liaison provided by Robert Olsen. Data reduction and report preparation were partially funded by the FY88 Research, Development, Test, and Evaluation (RDTE) Methodology Development Program.

SECTION 1. SUMMARY

1.1 BACKGROUND

In recent years there has been considerable interest in the measurement of atmospheric wind and turbulence using remote sensing techniques. Advances in electronics and in the understanding of atmospheric wave propagation have made possible the design of remote sensing instruments that utilize the interaction of acoustic or electromagnetic waves with turbulent density discontinuities in the atmosphere as a means of measuring wind and turbulence. The optical scintillometer is one class of relatively inexpensive instruments designed for remote wind and turbulence sensing. An optical scintillometer consists of a transmitter using a modulated 0.94-μm light-emitting diode (LED) source and a downrange receiver. The transmitter and receiver are aligned to form an optical path over distances of several hundred meters to several kilometers. Scintillometers use the scintillation of the irradiated energy to measure the refractive index structure parameter C_N^2 and/or the wind component transverse to the optical path. The log-intensity variance of the irradiance (σ_t^2) of the received signal is used to calculate C_N^2. An analysis of the irradiance covariance from paired receiver apertures determines the transverse wind component.

A new type of scintillometer, the spatially-averaged filter scintillometer or crosswind scintillometer, was designed and built for U.S. Army Dugway Proving Ground (DPG) in 1986-1987 by Gerard Ochs and James Wilson of the National Oceanic and Atmospheric Administration Environmental Research Laboratories/Wave Propagation Laboratory (NOAA ERL/WPL). This scintillometer consists of multiple transmitter and receiver apertures that form spatial filters at discrete segments along the optical path sensitive to turbulent eddies crossing the optical path. The instrument operates as a crosswind profiler, measuring the cross-path component of the wind at five segments along its optical path.

Path-averaged wind measurements have many potential applications, some of the most obvious being crosswind measurements along runways, across gorges, or in steep or otherwise inaccessible terrain. Another possible application is in the support of flat-fire trajectory weapons testing. The effect of wind on flat-fire trajectories has been described by McCoy (1976). McCoy evaluated the deflection (df) of a projectile due to a crosswind (cw) acting along the trajectory according to the expression

$$df = cw(t-R/V) \qquad (1\text{-}1)$$

where t is the actual time of flight to the projectile's downrange position R and V is the projectile's downrange velocity component. The term (t-R/V) is called a "lag time" because it is the time difference between the actual flight time and the flight time to the same range in a vacuum. McCoy found that the deflection due to a crosswind is greatest along that part of the trajectory where the rate of change in lag time with respect to distance is greatest. For flat-fire trajectories, the rate of change is greatest over the first half of the trajectory, decreasing to zero at the target. McCoy also

found that the effect of range (along-trajectory) wind on the trajectory is relatively insignificant. These results suggest the need for a crosswind measurement system weighted towards the first half of the range.

Fixed-point wind measurements are not necessarily representative of crosswind effects along a ballistic trajectory. A cup or propeller anemometer measures only the wind passing through its location. Data from these point sensors are averaged over time under the assumption that a temporal average approximates an average over space. This assumption is often violated, particularly in situations were winds are influenced by trees, buildings, or terrain variations. Also, it is often not possible to place anemometers near the projectile trajectory without having them destroyed, or without otherwise interfering with testing. A final consideration is instrument response. A mechanical wind instrument gains or sheds energy to achieve equilibrium with the wind field, but it cannot respond adequately to turbulent eddies of scales smaller than its distance constant. This limitation, which degrades the instrument's measurement accuracy, can be significant near the ground or in strong turbulence conditions.

The crosswind scintillometer has the potential to overcome the limitations of mechanical wind sensors for near-surface crosswind measurements. A scintillometer can be oriented parallel to a projectile's path to measure the crosswind component without creating obstacles along the path. Because the scintillometer does not gain or shed energy with the wind, there are no distance constants or other instrument-related effects to degrade wind measurements. DPG conducted a field test of its crosswind scintillometer at the Main Front Gun Range of the U.S. Army Aberdeen Proving Ground (APG) in November 1987 to demonstrate the feasibility of using scintillometers to measure crosswind profiles during flat-fire ballistics testing. The results of these tests at Aberdeen Proving Ground, MD are discussed in this report.

1.2 INSTRUMENT DESCRIPTION

The crosswind scintillometer consists of transmitter and receiver optics and accompanying electronics mounted within water resistant cases. The transmitter uses an LED source radiating over two 29-by 40-cm Fresnel lenses. Alternating clear and reflecting stripes are used on the lenses to form zero-mean filters of 5- and 20-cm wavelengths. The receiver optics consist of a 29- by 40-cm Fresnel lens forming zero-mean filters of 5-, 10-, and 20-cm wavelength. The transmitter and receiver include sunshades to protect the lenses from direct exposure to sunlight, and rifle scopes for optical alignment.

Combinations of the scintillometer transmitter and receiver zero-mean filters define spatial filters sensitive to cross-path winds at segments along the optical path. The filters selected for this instrument are weighted for maximum sensitivity to the crosswinds at the 1/5, 1/3, 1/2, 2/3, and 4/5 path segments. Dials displaying signal strength and crosswinds at each of the five path positions are mounted on the back of the receiver. An analog voltage output proportional to the crosswinds is available for each path segment. The receiver also includes a calibration mode switch for checking the operational status of the electronics. Figure 1.1 shows the rear view of a receiver with

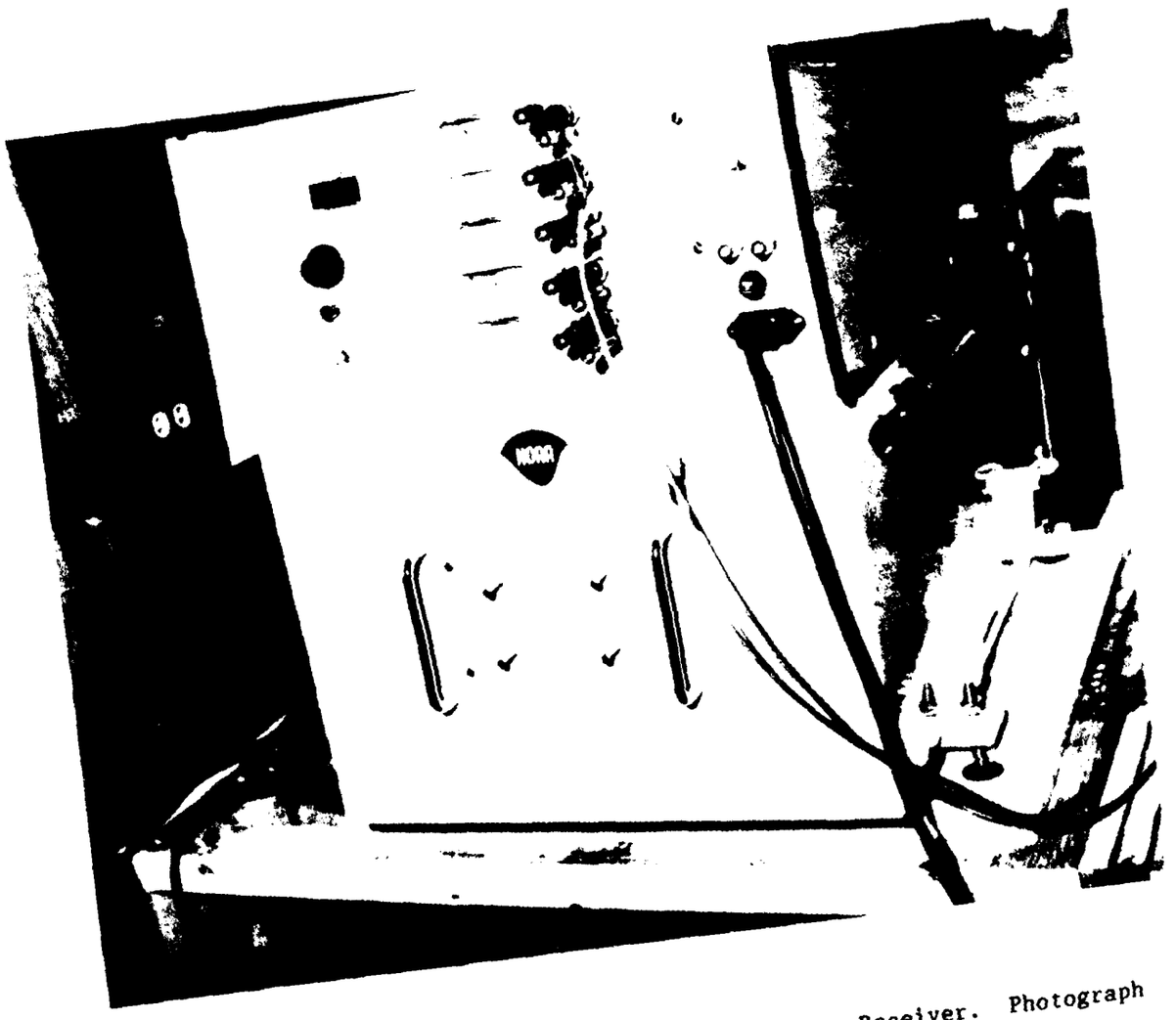

Figure 1.1. Rear View of the Crosswind Scintillometer Receiver. Photograph Courtesy of APG Audio-Visual Branch.

its signal strength meter, dials, rifle scope, calibration switch, and analog output dials.

1.3 TEST OBJECTIVES

The test objective was to demonstrate the applicability of the crosswind filter scintillometer to provide crosswind measurements at the APG Main Front Gun Range. Major questions addressed in this customer test for ASL were:

a. Optical Alignment. Can the scintillometers be easily aligned and will they maintain optical alignment in the presence of shock and vibration at the gun positions?

b. Reliability. Can the scintillometers operate reliably during field trials?

c. Adverse Weather. Will the instruments operate in rain and snow? Will they handle wind shifts across the optical path? Will they operate in high and low scintillation conditions?

d. Wind Measurement Precision and Correspondence. Do the scintillometers have precision equivalent to standard wind instruments? How well do scintillometer crosswind measurements correspond with crosswind measurements from other instruments?

1.4 RESULTS

a. Optical Alignment. Optical alignment must be established and maintained during field operation to obtain usable data from the crosswind scintillometer. Therefore, a major test objective was to determine if these instruments are sufficiently robust and easy to handle for field use. The scintillometers were shipped by land freight from Boulder, Colorado to APG and arrived in operating condition. Instrument setup, alignment, and operation proceeded without incident. Setup requirements were straightforward and did not require a great deal of time or expertise. The transmitter was placed on a stack of concrete blocks near the 1000-m target position, and the receivers were operated from the back of a 2-1/2 ton truck parked near the B-1 Barricade gun position. Optical alignment was easily established using the rifle scopes, with fine adjustments used to peak the signal strength meter. Scintillometer alignment and operation were not adversely affected by normal movement in and around the truck, or by shock and blast from nearby M-1 tank guns. The occasional passage of vehicles along the B1 line road caused intermittent blockage of the optical path and temporary loss of signal strength. However, this temporary loss of signal strength did not result in spurious crosswind measurements. In summary, the scintillometers survived shipment and were found to be easy to set up and operate in field conditions.

b. Reliability. The scintillometers operated continuously without failure throughout the test program. Calibration checks performed before each day's test detected no faults or failure modes.

c. Adverse Weather. The scintillometers were operated during adverse weather conditions, which included transition through sunset with low C_N^2 conditions and periods of rain and snow. Signal strength was unaffected when visibility was reduced to an estimated 2 km by light rain and snow showers. Low C_N^2 at sunset and during overcast conditions did not adversely impact scintillometer operation. There was no opportunity to test scintillometer operation in strong C_N^2 conditions during this test series. One trial was conducted during a period when the cross-path wind component repeatedly changed direction. The scintillometer generally tracked these wind reversals, but erroneous readings occasionally occurred. These errors occurred as the receiver servos lost their lock due to the absence of a predominant crossing wind component. This condition was self-correcting once a crossing wind component was reestablished. Periods of data loss due to loss of servo lock rarely exceeded 10 s. Path crossing performance problems are discussed in Section 2.4.5.

d. Wind Measurement Precision and Correspondence. Figure 1.2 shows the test site surface features and instrument locations. Scintillometer measurements were intercompared and compared with measurements by mechanical wind instruments and sonic anemometers. The test configuration included one scintillometer transmitter near the 1000-m target position and two receivers northwest of the B-1 Barricade. This configuration created two closely spaced, quasi-parallel optical paths. The crosswind measurements from segments along each optical path were compared using bias, comparability, and precision, as defined by Hoehne (1971). The results, presented in detail in Section 2.4.3, show a bias of 12 cm/s due to larger crosswinds measured by scintillometer Unit #3 than Unit #2. This bias could not be explained by environmental factors and probably represents a difference in instrument response. Precision, which does not include bias, was approximately 5 cm/s. These bias and comparability results compare favorably with the results of cup and propeller anemometer intercomparisons performed at the Boulder Atmospheric Observatory (BAO) by Finkelstein et al. (1986).

Scintillometer data were also compared with data from the ASL GMQ-11 aerovanes and DPG sonic anemometers. Comparisons were possible only with the aerovanes at the 200- and 700-m positions because the aerovane at the 400-m position failed early in the test series, producing insufficient data for a meaningful intercomparison. The DPG sonic anemometers set up at the 600-, 662-, 830-, and 919-m positions were used in the comparisons. The mean crosswinds were compared for each trial, and the crosswind standard deviations were compared to examine instrument response to wind variability. The scintillometer crosswind measurements were generally found to be comparable to the crosswinds obtained from the fixed-site instruments, but exhibited a slight bias toward lower speeds. This bias can be partly explained by instrument calibration, operating characteristics, and data processing techniques (see Section 2.4.2), but an adjustment of the scintillometer calibration constant may also be required. Instrument performance using a variety of measures indicated that the scintillometers tracked the crosswinds well in a complex and variable wind field.

1.5 CONCLUSIONS

Field tests at the APG Main Front Range demonstrated that the crosswind scintillometer is a robust, reliable, and easy to use under field conditions. Also, the scintillometer is sufficiently portable for movement between test sites. Scintillometer accuracy was found to be comparable to that of high quality mechanical anemometers. The scintillometer successfully produced crosswind information of the quantity and quality required for the testing of flat-fire trajectory weapons. Although the scintillometer's operation was not adversely affected by light precipitation, it would probably fail in thick fog, heavy rain, or snow because of signal attenuation.

The major problem identified during the scintillometer test occurred with light and variable wind conditions when frequent wind reversals created ambiguities in the sign of the crosswind component. Adjustment of the lags in the wind-speed and crosswind direction circuitry is needed to correct this condition. Further testing is also needed to better define the scintillometer calibration factor.

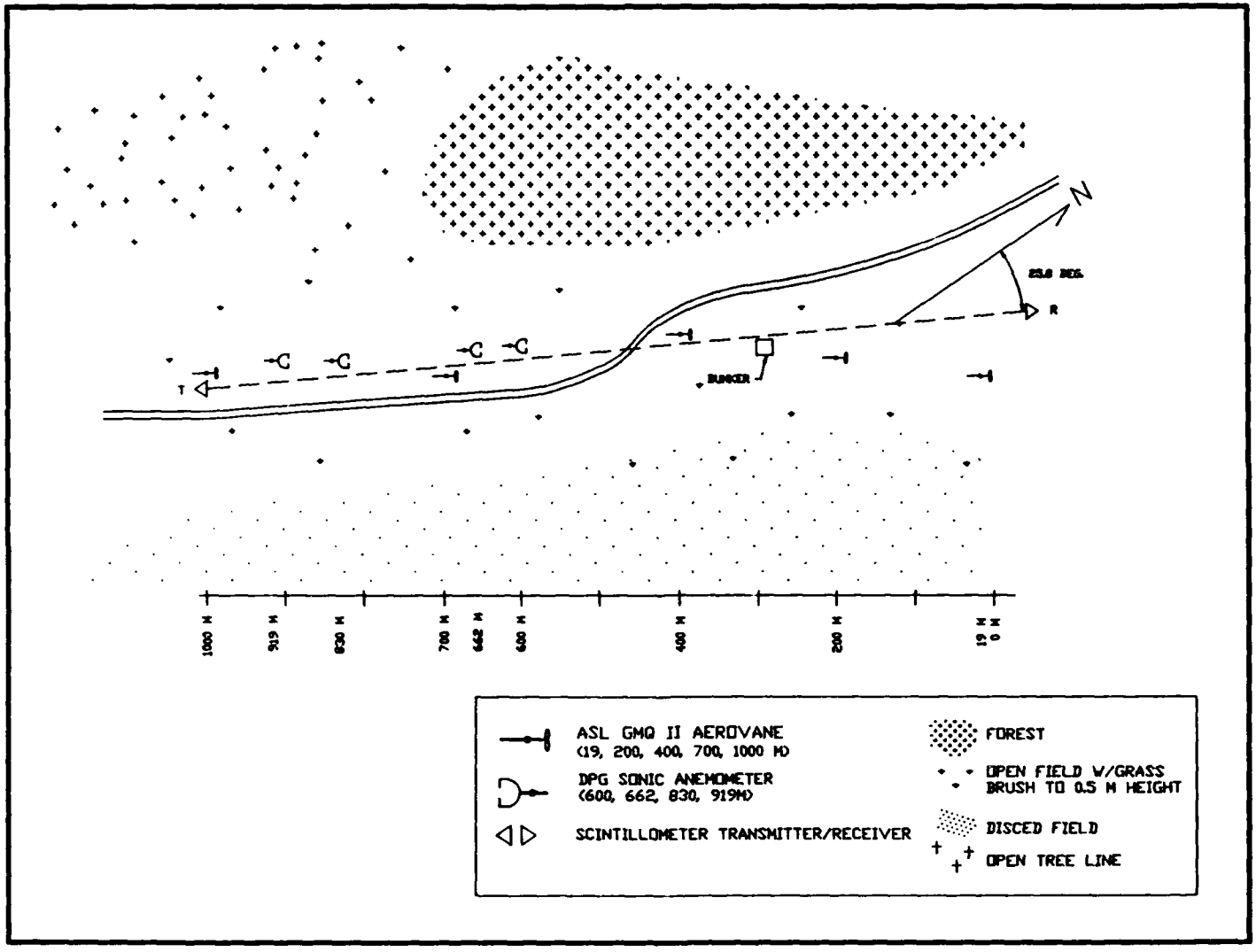

Figure 1.2. Overview of APG Main Front Gun Range Anemometer Line with Locations of Major Instruments and Surface Features.

The scintillometers used in the APG trials are prototypes designed for use in smoke/obscurant testing. Different design considerations (for example, different path weighting functions) and different operational path lengths may be more applicable for gun range crosswind measurements. Nevertheless, the results of this test indicate that the crosswind measurement requirements at the APG Main Front Range could be easily satisfied with the installation of a scintillometer receiver on top of a berm separating the gun positions and the transmitter on a downrange berm. In this configuration, the optical path would be quite close to the trajectory of a flat-fire test round, and the scintillometer could provide representative crosswind data without interference with the round.

INTENTIONALLY BLANK

SECTION 2. DETAILS OF TEST

2.1 CHARACTERIZATION OF SITE AND WEATHER CONDITIONS

2.1.1 Site Description

The scintillometer test was conducted at the anemometer line along the western edge of the APG Main Front Gun Range. This range is located on the west shore coastal plain of the Chesapeake Bay. The portion of the anemometer line used in these tests extends from the B-1 Barricade to the 1000-m target position. Side and top views of the B-1 anemometer line are shown in Figures 2.1 and 1.2, respectively. An asphalt/gravel service road extends along the line and crosses it at 470 m downrange. Because of a slight rise in terrain, the road is 1 to 2 m below grade from 570 to 720 m downrange. Site elevation ranges from 9 m above mean sea level (MSL) near the 200-m anemometer position to 11.5 m MSL near the 700-m anemometer position, and 10.5 m MSL at the 1000-m position (see Figure 2.1).

Winds at the B1 anemometer line are dominated by the Bay breeze and a prevailing northwesterly flow. A major feature influencing local wind conditions along the anemometer line is a dense stand of trees that extends from north of the B-1 Barricade to the 700-m position (see Figure 1.2). The tree line is 30 to 50 m west of the road and anemometer line. These trees are typical of central hardwood forests, consisting of a mixture of black tupelo, black oak, red maple, sweet gum, and white oak. The average crown height is 14 m. Although virtually all the leaves had fallen off prior to the November tests, the thickness of the stand presented a significant blockage to winds from the west through northwest. The field east of the tree line and the areas along the anemometer line and the road contain relatively undisturbed grass and brush 0.5 m or less in height. A 1-km wide disced field located 20 m east of the anemometer line serves as the firing fan for the Main Front Range. These features are shown in Figure 1.2.

Insufficient time was available to make detailed site roughness measurements, but the roughness length z_o is estimated to be between 2 and 5 cm for a fetch across the open field and between 0.2 to 0.5 m for the fetch through the trees. The tree line created a complex micrometeorological setting for west through north winds. The change in surface roughness between the tree line and the open field caused the formation of a new turbulence sublayer in the lee of the tree line. Although analysis of this sublayer is beyond the scope of this report, it presented the opportunity to compare the performance of optical, sonic, and mechanical wind instruments in a non-ideal, "real world" setting.

2.1.2 Trial Winds and Weather

The 4-min averaged GMQ-11 aerovane wind data collected during the trial on 19 through 21 November 1987 were used to characterize trial wind conditions. Data were collected on 19 November from 0855 to 1550 Eastern Standard Time (EST), on 20 November from 0945 EST to 1725 EST, and on 21 November from 0830 EST to 1115 EST. These data collection periods were punctuated with breaks to change cassette tapes and to perform other miscellaneous work on the

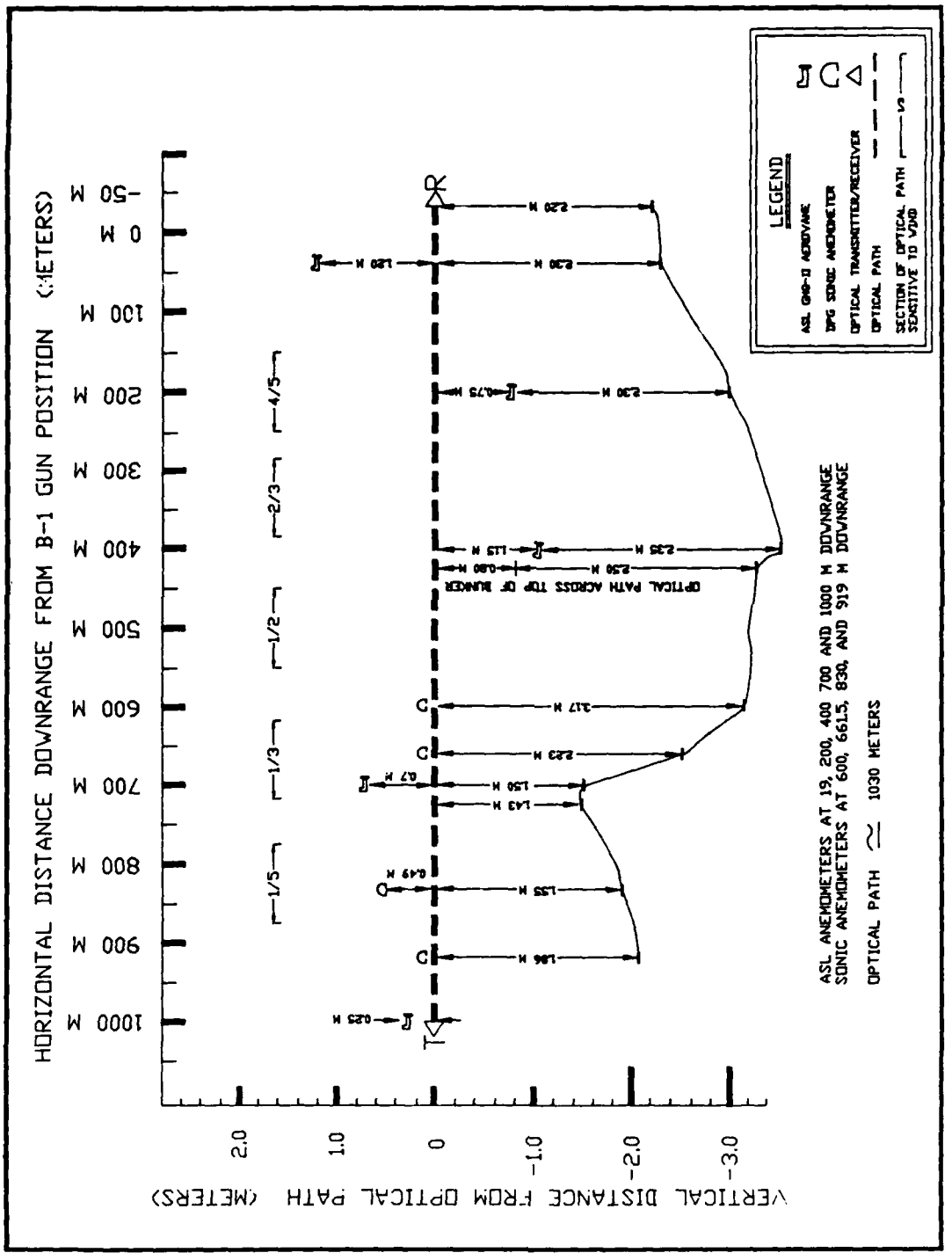

Figure 2.1. Cross Section of APG Main Front Gun Range Anemometer Line with Locations of Major Instruments and Terrain Heights with Respect to the Optical Path.

test site. Within these operating times, five trial periods labeled SCNT2 through SCNT6 were chosen for detailed analyses. These trial periods are summarized in Table 2.1. Scintillometer data were lost during Trial SCNT4 when the cassette ran out of tape.

Table 2.1. APG Scintillometer Trial Periods.

Trial Name	Date	Trial Time (EST)		Data Availability[a] Scintillometer		Sonic Anemometer			
		Start	Stop	Unit #2	Unit #3	919m	830m	660m	600m
SCNT2	19 Nov	1228	1436	Y	Y	Y	Y	Y	Y
SCNT3	20 Nov	0951	1116	Y	Y	Y	Y	Y	Y
SCNT4	20 Nov	1332	1428	M	M	Y	Y	Y	Y
SCNT5	20 Nov	1510	1705	Y	Y	Y	Y	Y	Y
SCNT6	21 Nov	0931	1022	Y	Y	M	Y	Y	Y

[a] Y=data available, M=data missing.

One test objective was to evaluate the crosswind scintillometer under both favorable (steady cross-path winds) and unfavorable (variable along-path winds and adverse weather) conditions. Figure 2.2 shows a polar plot of the ratios of the 200 m position GMQ-11 wind speeds to the 700-m position GMQ-11 speeds versus the corresponding 700-m position GMQ-11 wind directions. A ratio of 1.0 is indicated by the circle, with tick marks provided for the 0.5 and 2.0 ratios. There is no horizontal wind shear when the wind-speed ratio is 1.0. The scintillometer optical path, with an orientation of 026°, is included for reference. The open circles in Figure 2.3 represent winds for the trial on 19 November. The variable along-path winds on 19 November were very unfavorable for crosswind scintillometer measurements because they made multiple cross-path wind reversals and produced weak crosswind signal strengths. The effects of these unfavorable conditions on scintillometer performance are discussed in Section 2.4.5. Steady winds with strong crosswind components on 20 and 21 November, (represented in Figure 2.2 by diamonds and squares, respectively) provided ample signal strength for crosswind scintillometer operation. (Much of the apparent scatter in the 20 November data is due to northwesterly winds during the morning trial and westerly winds during the afternoon trial.) Thus, the objective of testing the scintillometer under both favorable and unfavorable wind conditions was achieved.

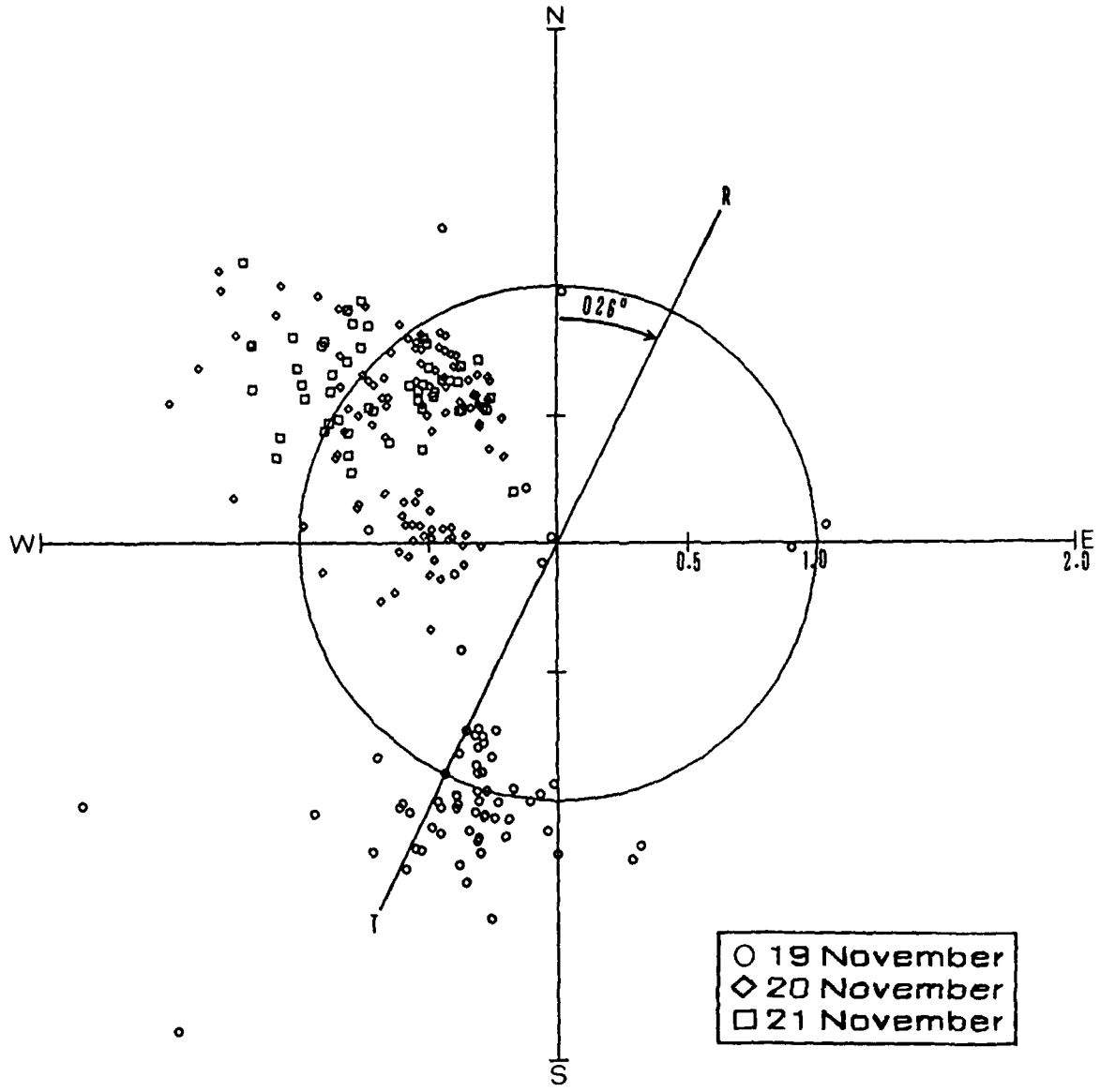

Figure 2.2. GMQ-11 wind speed ratios formed from 4-min averaged 200/700 m wind speeds plotted by 700 m averaged wind direction on days 19, 20, and 21 November 1987. Line T-R depicts the crosswind scintillometer optical path orientation with respect to the wind field.

As shown by Figure 2.2, the 200/700-m wind speed ratios on 20 and 21 November varied as a function of wind direction. Westerly winds, which provided an open fetch to the 700-m GMQ-11 position, passed through the tree line before reaching the 200-m GMQ-11 position. The resulting 200/700-m wind-speed ratio of approximately 0.5 means that the tree line removed up to half of the momentum of the near-surface wind reaching the 200-m position. As the wind direction veered towards the northwest, the 700-m GMQ-11 position was also sheltered by the tree line and the wind-speed ratios increased accordingly. The wind-speed ratios in excess of 1.0 are interpreted as evidence of a more severe blockage at the 700-m position than at the 200-m position. The shadowing occasionally extended to the 1000-m anemometer position when the winds were northerly. Data from the 400-m GMQ-11 position were missing for most of the test series. However, the little data that are available suggest that the mid-path winds were well sheltered for all for westerly wind components.

The crosswind scintillometers were also operated during adverse weather, which included precipitation and low C_N^2 conditions. The 20 November trials occurred during light rain showers which began at 1145 EST and continued intermittently throughout the afternoon in a prefrontal synoptic situation. By late afternoon, it was overcast with intermittent light rain and gusty winds, producing low (but unmeasured) C_N^2 conditions. The scintillometers performed throughout this period without difficulty. An overnight frontal passage dropped temperatures well below zero degrees Celsius, and the data collection period on 21 November was characterized by low C_N^2 in overcast conditions with intermittent light snow. Visibilities were occasionally reduced to 2 km in snow, but the scintillometers continued to perform without a detectable loss of signal strength.

2.2 INSTRUMENTATION

2.2.1 Introduction

Instrumentation used during the test series included GMQ-11 aerovanes at fixed positions along the anemometer line, sonic anemometers mounted on temporary masts, and two scintillometer receivers with one transmitter, forming two quasi-parallel optical paths. The ASL-operated GMQ-11s are the instruments currently used for meteorological support to ballistics testing at the Main Front Range, while the DPG-supplied sonic anemometers are designed for micrometeorological wind and turbulence measurements. The optical paths and sonic anemometer positions are shown in Figures 2.1 and 1.2. Because of the vertical wind-speed gradient, vertical separation of the fixed-site instruments from the optical path was a major concern. Given the physical constraints of the test site, sonic anemometers were positioned as close as possible to the optical path. The following subsections describe each type of instrument and the limitations on its performance during the crosswind scintillometer tests.

2.2.2 GMQ-11 Aerovane

The U.S. military's nomenclature for the ASL wind instruments deployed along the B-1 anemometer line is: Transmitter, Wind Direction & Speed, T-420(A)/GMQ-11. These instruments are representative of aerovane transmitter

designs offered by several manufacturers. The GMQ-11 aerovane consists of a 6-blade propeller of 39-cm diameter, mounted on the front of an aerodynamic housing 84 cm in length that acts as a wind vane. This transmitter assembly weighs 4.5 kg. The GMQ-11 provides output voltages proportional to wind speed and direction. Aerovanes are calibrated by applying a known rotation rate to the impeller rotor and monitoring the voltage.

Figure 2.3 shows the GMQ-11 aerovane located at the 1000-m position; the scintillometer transmitter inside a protective housing is at its left. GMQ-11 aerovanes are also located at positions 19, 200, 400, and 700 m downrange from the front of the B1 barricade (see Figures 2.1 and 1.2). The measurement heights range from 2 to 2.5 m above ground level. Data from the 200-, 400-, and 700-m anemometers were relevant to the optical scintillometer test, but data from the 400-m GMQ-11 were unavailable.

GMQ-11 data were sampled at a rate of once every 5 s during trial periods. The data were output on a thermographic tape in a printing process that takes approximately 15 s. In addition to wind data, pressure, temperature, humidity, and other thermodynamic variables were printed for each averaging interval. Because of the slow sampling rate and the lack of sampling during the printing process, this data system was set to its maximum averaging period of 4 min, (240 s) resulting in a complete data collection and print cycle of 255 s. Only the GMQ-11 mean wind speeds and wind directions were used in this study. The site and performance considerations described in Appendix C suggest that the GMQ-11 aerovanes deployed along the B-1 anemometer line have an overspeed bias of 5 to 10 percent.

2.2.3 Sonic Anemometer

Four DPG sonic anemometers were positioned along the anemometer line (see Figure 1.2). These instruments were RSWS-201/2A two-axis sonic anemometers manufactured by Applied Technologies, Inc. (ATI). The RSWS-201 consists of paired orthogonal sets of acoustic transmitter/receivers with a transducer separation distance of 15 cm. Microprocessor circuitry counts intervals of time between transmission and reception of sound pulses at the transducers. The sample rate is 200 Hz, with measurements averaged to 10 Hz and output in an RS232 ASCII serial data stream. The DPG version of these instruments has been modified to produce an analog $\pm$10V direct current (DC) output corresponding to $\pm$100 m/s. Sonic anemometer performance considerations, described in Appendix D, suggest a measurement uncertainty of 5 percent, including a possible overspeed bias.

The sonic anemometers were mounted on masts with their heights adjusted for proximity to the height of the optical path. Figure 2.1 documents the vertical separations of the sonic anemometers from the optical path. A sonic anemometer mounted in an inverted configuration for proximity to the optical path is shown in Figure 2.4. The boom arms holding the sonic anemometers were leveled and oriented uprange towards the scintillometer receivers, so cross-path wind components were measured by the sonic anemometer v-axis. Because insufficient instrumentation was available to place sonic anemometers along

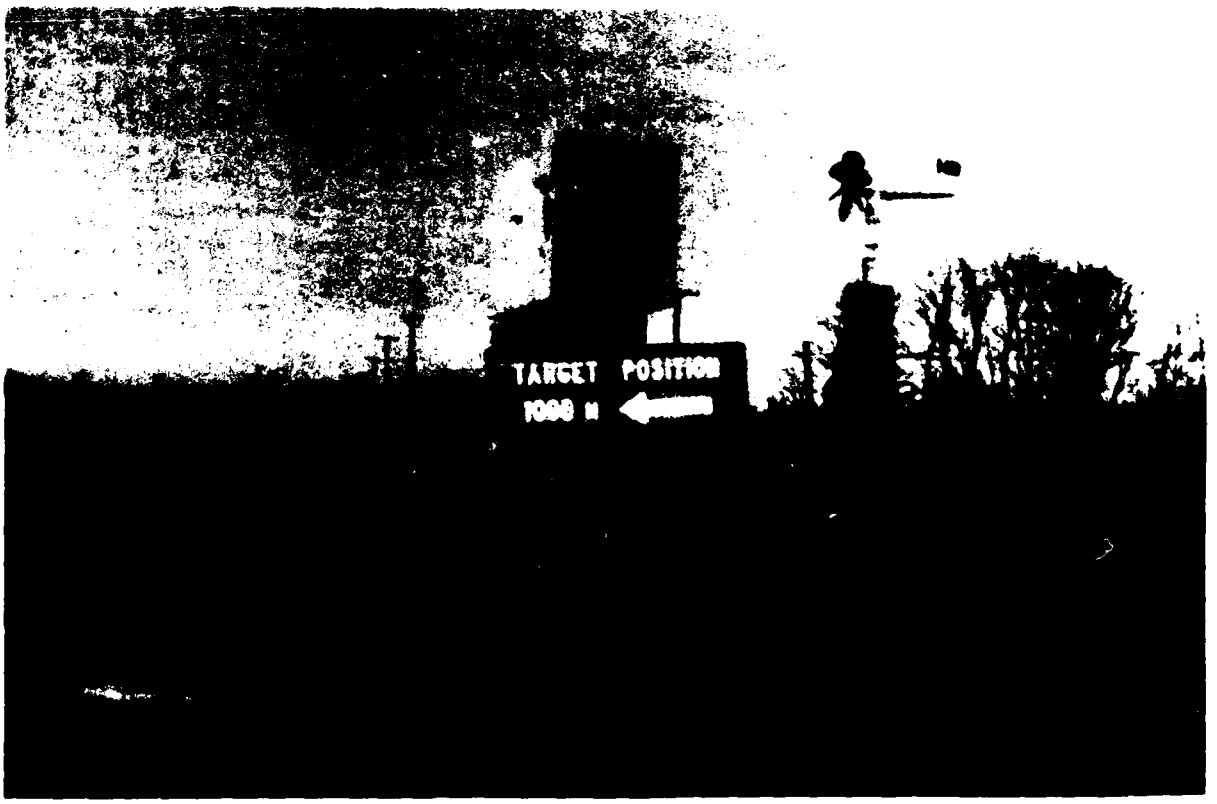

Figure 2.3. Crosswind Scintillometer Transmitter in a Protective Housing, and GMQ-11 Aerovane Located at the 1000-m Downrange Position, APG Main Front Gun Range Anemometer Line. Photo Courtesy of APG Audio-Visual Branch

the entire optical path, the sonic anemometers were concentrated at the transmitter end of the path to better document the treeline induced crosswind shear. Analog data from the sonic anemometers were recorded at a 2 Hz rate on Campbell Scientific CA21X data loggers.

2.2.4 Crosswind Scintillometer

The crosswind scintillometer consists of a transmitter and a downrange receiver, with an optical path established between the two. A general description of scintillometer operation is presented in Appendix A. The crosswind scintillometer transmitter uses an LED source radiating over a 1.8-mm diameter hemisphere with a ground glass diffuser to enlarge its radiating area. Two 29- by 40-cm Fresnel lenses with alternating clear and reflecting stripes form zero-mean filters (d_t) of 20- and 5-cm wavelengths. Receiver optics consist of one 29- by 40-cm Fresnel lens forming three pairs of zero-mean filters (d_r) of 5-, 10-, and 20-cm wavelengths. Ratios of the transmitter and receiver zero mean filter wavelengths define spatial filters of wavelength w transverse to the optical path. These spatial filters define

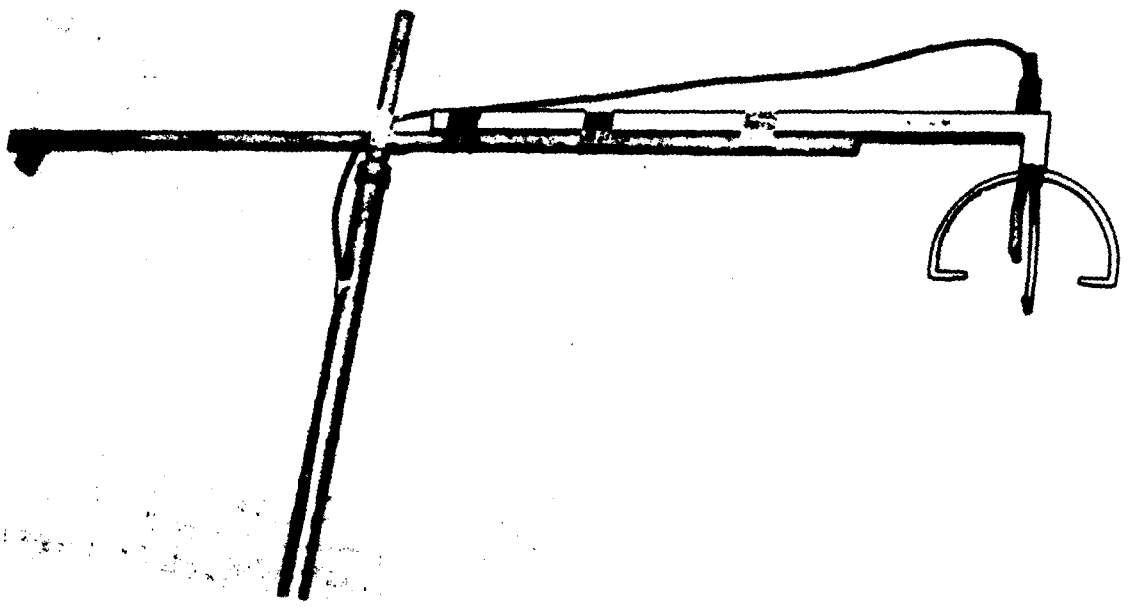

Figure 2.4. Two-axis Sonic Anemometer Head Mounted in an Inverted Configuration. Photo Courtesy of the APG Audio-Visual Branch.

the sizes of turbulent eddies that contribute the strongest signals to the receiver from each path position. The relationships between zero-mean filter element size, path position, and spatial wavelength are presented in Table 2.2. These relationships are defined by Ochs et al. (1988) as

$$z = L/(1 + d_r/d_t) \tag{2-1}$$

and

$$w = d_r d_t/(d_r + d_t) \tag{2-2}$$

where z is the distance from the transmitter to the center of the weighting function peak and L is the optical path length.

Table 2.2. Relationship Between Zero-Mean Element Size, Path Position, and Spatial Wavelength.

Zero-Mean Filter		Path	Spatial
Transmitter	Receiver	Position	Wavelength
d_t (cm)	d_r (cm)	z/L	w (cm)
5	20	1/5	4.00
5	10	1/3	3.33
5	5	1/2	2.50
20	10	2/3	6.67
20	5	4/5	4.00

Crosswind speed and direction are obtained from the correlation and covariance of signals received from each of the spatial filters. An atmospheric eddy carried by the wind across a spatial filter can generate a fluctuating signal at the receiver. The frequency of this signal is defined by the ratio of the translation speed to the spatial wavelength of the filter. Time-lagged autocorrelation functions define crossing times and hence translation speeds. Crossing direction is defined by measurement of normalized signal covariances at 14 time lags. Lag measurements are made on signal covariance functions displaced both positively and negatively in the horizontal direction. Summations of the biased signals (positive if time lags are short relative to signal covariance, negative if time lags are long relative to signal covariance) are used in a servo loop to adjust shift register delay until the summation is zero. The sign of the servo voltage determines the direction of crossing. The sign convention used in these scintillometers is for a positive voltage (positive crosswind) when scintillation patterns cross from left to right as viewed from the receiver.

For the spatially-averaged filter design used in the crosswind scintillometer, there is a design tradeoff between sharp path weighting functions (small d, small spatial wavelength) and saturation effects, which are greater for smaller d. Element sizes of 5, 10, and 20 cm were chosen as a compromise between the desired sharp weighting function and the avoidance of saturation. The range of this crosswind scintillometer is limited to distances on the order of 1 km because of the increase in saturation effects with distance and the decrease in the signal-to-noise ratio to unacceptable levels. Figure 2.5 shows the path weighting functions calculated by NOAA ERL/WPL (Ochs et al, 1988). The ordinate in Figure 2.5 represents the relative sensitivity of the spatial filters to winds transverse to the optical path. The sharpness of the weighting functions is inversely proportional to the magnitude of spatial wavelengths presented in Table 2.2.

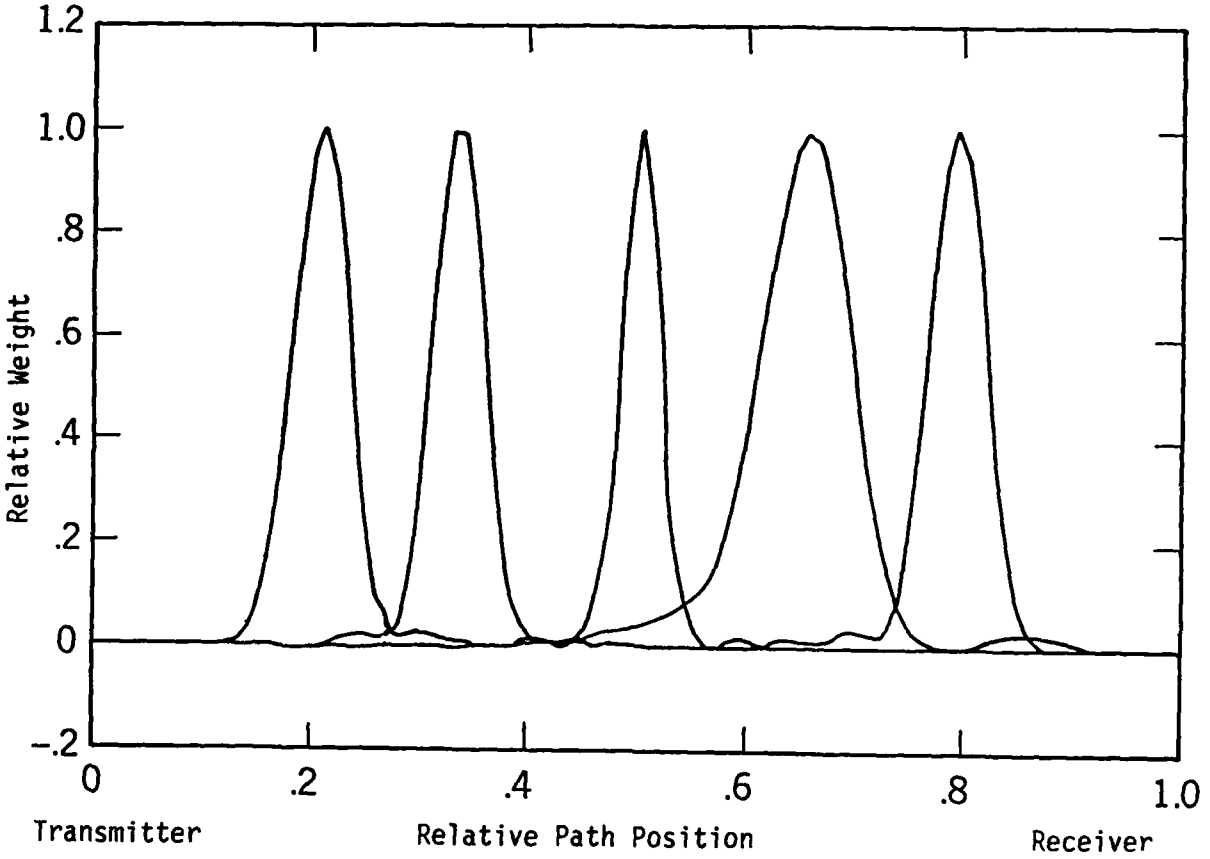

Figure 2.5. Calculated Path Weighting Functions (Ochs et al., 1988).

The normal deployment configuration for a crosswind scintillometer is a single transmitter-receiver pair forming an optical path. For the APG test series, one transmitter at the 1000-m target position was used to form two quasi-parallel optical paths with two receivers, Unit #2 and Unit #3, stationed in the back of a 2 1/2-ton truck near the B-1 Barricade. This configuration permitted a direct comparison of receiver performance and minimized downrange equipment setup.

Data from the crosswind scintillometers were previously compared with data from fixed-point anemometers in a calibration study at a flat, open site on Table Mountain near Boulder, Colorado (Ochs et al., 1988). The fixed-point instruments used as a calibration reference were UVW Model 27106 propeller anemometers manufactured by the R. M. Young Company. These propeller anemometers are calibrated by applying a known rotation rate to the propeller rotor and monitoring the output. A threshold near 0.2 m/s and a distance constant of 0.74 m makes these instruments suitable for micrometeorological measurements. Response of the UVW anemometer series instruments is well documented (Camp et al., 1970; Finkelstein et al., 1986).

Ochs et al., (1988) determined crosswind scintillometer calibration from

$$cw = Kfw, \qquad (2\text{-}3)$$

where cw is the cross-path wind component measured by the UVW anemometers, f is the mean measured frequency, w is the spatial wavelength at each path position, and K is the calibration factor. Ochs et al. found K to be 0.83. This calibration factor is necessary because of medium decorrelation. Medium decorrelation occurs because eddies decay as they translate across the optical path. Medium decorrelation shifts the covariance peaks used to define wind speed towards a shorter delay, which translates to a higher wind speed. The K factor of 0.83 is an approximation that is likely to vary as a function of the angle of the wind with respect to the optical path, decreasing further from unity as the wind direction becomes more parallel to the optical path. An uncertainty on the order of ±5 percent is anticipated for K until additional calibration tests are performed.

At the start of the crosswind scintillometer test at APG, there was some concern that atmospheric density affected the UVW anemometer response, and hence the crosswind scintillometer calibration factor, during the Ochs et al. (1988) study. That is, use of a K defined at an elevated site could introduce a significant bias in the measurements made during the APG test. However, Gill (1973) concluded that the response of helicoid propellers, as used on the UVW anemometers and aerovanes, are virtually independent of atmospheric density over its normal range. Consequently, it was subsequently assumed that site atmospheric density differences do not influence K.

2.3 DATA COLLECTION AND REDUCTION PROCEDURES

Data from the sonic anemometers and crosswind scintillometers were recorded at 2 Hz on three battery-operated Campbell Scientific CA21X Micrologger data loggers. The data logger manufacturer's specifications include fourteen-bit precision and 1.2-μv root-mean-square (RMS) noise. High level voltage signals (on the order of several volts) from the sensors were transmitted via cable to the Microloggers. One Micrologger was used to record 10 channels of data from the scintillometer receivers located in the rear of the 2 1/2 ton truck, a second Micrologger was used to record u and v wind component data from the 600- and 660-m sonic anemometers (4 channels), and the third Micrologger was used to record u and v data from the 830- and 919-m sonic anemometers. Analog data line losses were judged to be insignificant, and there was no evidence of ground loops or radio frequency (RF) noise.

The programmable Microloggers permitted the field conversion from analog voltage signals to engineering units. Data in engineering units were stored on cassette tapes by connection through an SC92 Interface Connector and Radio Shack audio recorder. Data on the cassette tapes were spot checked after each day of testing to ensure that good quality data were being collected.

Data from the cassette tapes were processed via an RS232 port through an interface box into a DEC Rainbow™ 100 personal computer. Next, the data were electronically transferred to a PDP 11/44 computer to create an ASCII

text file. This file was then electronically transferred through a DECNET™ or ETHERNET™ link to the DPG VAX™ 8800 cluster system and processed into the DPG RETRIEVE system for user access. Data were taken from the RETRIEVE system for further reduction and analysis using the MEBSFLXVAR and MEBSRAWSPC programs to produce means, variances, and spectrum information.

Random data loss due to tape read errors was observed. Tape read errors appeared as zeroed data fields for all channels on each affected 0.5-s time record. These tape read errors, which caused a loss of 3 to 4 percent of the data, were randomly distributed and rarely occurred in adjacent time records. Following the recommendations of Koopmans (1974), each tape read data gap was filled using the average of data from the records immediately preceding and following the gap. This procedure was required to provide a continuous record for spectrum analysis of the time series data. A review of the records showed that no major data collection system failures occurred, although data were sometimes lost when the cassette ran out of tape or if the Micrologger was inadvertently not turned on.

2.4 QUANTITATIVE ANALYSIS

2.4.1 Introduction

Several measures were used to evaluate scintillometer crosswind performance. Analyses were performed using three time series data sets: the GMQ-11 data, the sonic anemometer data, and the scintillometer data. The GMQ-11 data have a small sample size because of their data collection system's slow data rate. Consequently, these data were used only for test site wind characterization (Section 2.1.2) and mean crosswind intercomparisons. The sonic anemometer and scintillometer data, collected at a 2 Hz rate, were subjected to additional analyses. Section 2.4.2 contains a comparison of mean scintillometer-derived crosswinds with crosswinds obtained from the sonic anemometers and GMQ-11 aerovanes. Mean scintillometer crosswind data were also used for scintillometer receiver performance intercomparison using bias, comparability, and precision measures (Section 2.4.3). Time averaging effects on turbulence scale measurements are presented in Section 2.4.4, and scintillometer crosswind measurement problems with variable cross-path wind directions are discussed in Section 2.4.5. Section 2.4.6 is devoted to an analysis of sonic anemometer and scintillometer spectra, including line averaging effects and other comparison measures.

2.4.2 Mean Crosswind Comparisons

A comparison was made of crosswind readings from the three measurement systems. Cross-path wind components were initially computed for the 4-min averaged GMQ-11 data. The GMQ-11 crosswinds were then averaged into 20-min blocks for comparison with 20-min averaged sonic anemometer and crosswind scintillometer winds. Data from 20 November only were used for this purpose because variable crosswinds on 19 November caused scintillometer performance problems (see Section 2.4.5), and the 919-m sonic anemometer malfunctioned on 21 November. What remained were seven 20-min data blocks on 20 November where all instruments except for the 400-m GMQ-11 were generating relatively error-

free data. These block-averaged crosswinds were again averaged to produce the mean crosswind speeds shown at the various optical path measurement positions in Figure 2.6.

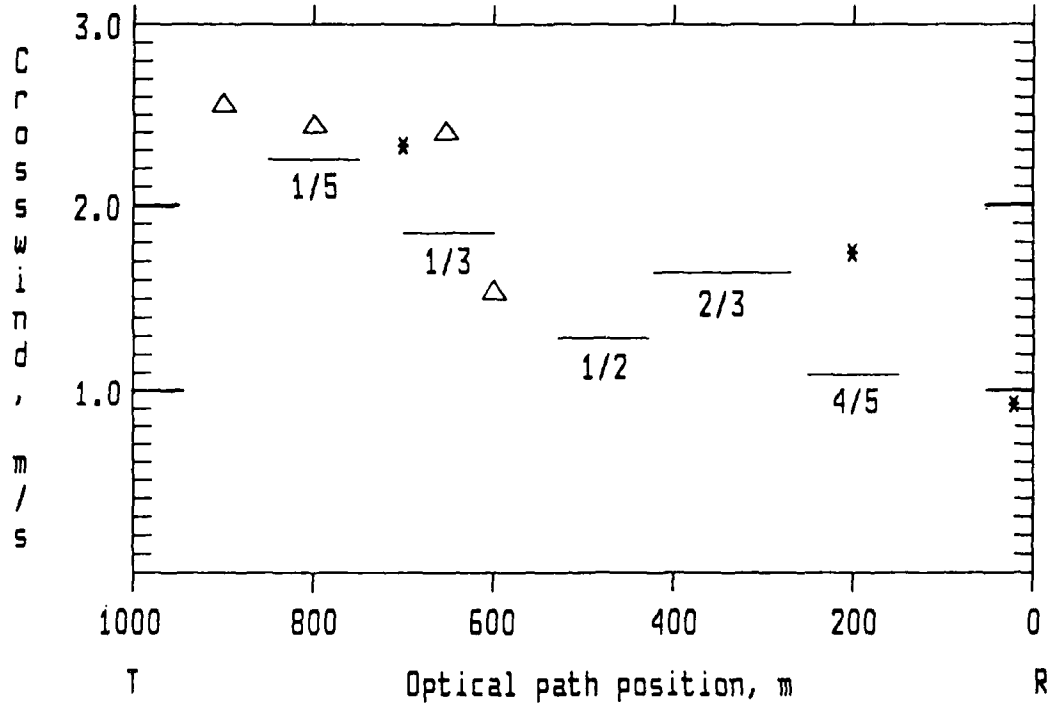

Figure 2.6. Mean Crosswind Speeds from Sonic Anemometers (Δ), GMQ-11s (*), and from the Indicated Scintillometer Path Segments (——). T Represents the Scintillometer Transmitter Position, and R Represents the Scintillometer Receiver Positions.

Figure 2.6 illustrates an abrupt decrease (or shear) in mean wind speed between the 660-m (~2.5 m/s) and 600-m (~1.5 m/s) sonic anemometer positions caused by the tree line. The 1/3 scintillometer path segment crosswind appears to be an average over this shear zone. The differences in the 1/2, 2/3, 4/5 path-segment crosswinds, and the 200-m GMQ-11 crosswind indicate the presence of other tree-line induced shear effects as well. (Figure 2.6 also illustrates some of the difficulties in making representative wind measurements in a complex wind field.) Although the scintillometer crosswinds indicate the same general trend in the wind field as the fixed-point sensors, individual differences between path-segment and point-sensor measurements are difficult to reconcile. The mean crosswinds measured at the 1/5 path segment is 11 percent lower than the average of the 919- and 830-m sonic anemometer mean crosswinds. Similarly, the 1/3 path position mean crosswind is 6 percent lower than the average of the 660- and 600-m sonic anemometer crosswinds. Given the uncertainties inherent in wind-speed measurements and the variability in the wind measurements along this path, this correspondence is quite good. On the other hand, the 4/5 path position scintillometer crosswind is 37

percent lower than the 200-m GMQ-11-derived crosswind. Many more fixed point anemometers would be needed along the optical path to fully evaluate scintillometer mean wind measurements in this complex wind field.

Wind measurement accuracy is bounded on one side by statistical uncertainty due to small sample size and on the other by the presence of trends and spatial inhomogeneities. These factors limit the degree of certainty to which a true ensemble mean crosswind can be approximated by time-averaged measurements. An ensemble mean crosswind is defined over both time and space. Measurements made in a turbulent wind field that is statistically invariant (i.e., contains no trends or spatial inhomogeneities) can approach the ensemble mean. A useful consequence of statistical invariance is that time-averaged and space-averaged measurements become essentially equivalent. Statistical invariance is implicitly assumed when time-averaged data from fixed-site wind instruments are used to measure the mean wind. Assuming statistical invariance, the averaging time (t) required to determine a mean wind speed ($\bar{u}$) to an accuracy ε is given by Lumley and Panofsky (1964) as

$$\bar{t} \simeq 2 \frac{\bar{u}'^2 \tau}{\bar{u}^2 \varepsilon^2} \qquad (2\text{-}4)$$

where $\bar{u}'^2/\bar{u}^2$ is the ratio of variance to the square of the mean wind speed and τ is the integral time scale of u. The integral time scale is the time interval required to obtain an independent measurement from each major turbulent element contributing to the mean wind. Following Wyngaard (1973), τ for a fixed-site sensor is approximated by the ratio of the dominant turbulence scale length ( ) to $\bar{u}$. For near-surface wind measurements, is roughly equivalent to height above the surface. The fixed-site wind measurements at the APG scintillometer trials were made near 2 m AGL in 2 m/s winds, producing a τ of 1 s. The scintillometer, on the other hand, obtains crosswind readings as an average from many turbulence elements along the optical path. For a path segment length of 100 m and a dominant turbulence scale of 2 m, the scintillometer path-averages crosswinds over 50 eddies for each measurement. This produces an equivalent integral scale that is one fiftieth of the fixed-site sensor integral scale. A 2t of 40 s is required for a point sensor to obtain an ε of 5 percent when u'^2/u^2 is 0.05. The scintillometer can achieve the same degree of accuracy in 0.8 seconds. The reader should note that the foregoing figures are based only on statistical considerations. In practice, scintillometer data are averaged over a period of at least one second.

2.4.3 Scintillometer Bias, Comparability, and Precision

The test design with two nearly parallel scintillometer paths permitted an intercomparison of scintillometer receiver performance using bias (b), comparability (c), and precision (s), as defined in Hoehne (1971). Bias, the average inter-instrument difference, is given by

$$b = \frac{1}{N} \sum_{i=1}^{N} (CW_{wi} - CW_{ei}) \qquad (2\text{-}5)$$

where N is the sample size, CW_{wi} is the ith crosswind measured along the optical path established by the transmitter and the west scintillometer (Unit #3), and CW_{ei} is the ith crosswind measured along the east scintillometer (Unit #2) path. Comparability is the RMS measurement difference, given by

$$c = \left[\frac{1}{N} \sum_{i=1}^{N} (CW_{wi}-CW_{ei})^2\right]^{1/2} \qquad (2\text{-}6)$$

Precision, defined as the standard deviation of the measurement differences, is obtained from

$$s = [c^2 - b^2]^{1/2} \qquad (2\text{-}7)$$

Table 2.3 summarizes the bias, comparability, and precision computed using 255-s averaged scintillometer crosswind data; the five trials were 51 to 128 min long. Systematic biases are apparent in the crosswind measurements because Unit #3 measured consistently lighter crosswinds ((CW_w-CW_e) negative) than Unit #2 at the 1/5 and 1/3 path positions, but consistently stronger crosswinds ((CW_w-CW_e) positive) at the 2/3 and 4/5 path positions. The bias is at a minimum for the 1/2 path position. This pattern is consistent for all trials and is therefore not an obvious function of wind or weather conditions. The cross-path wind measurement problems described in Section 2.4.5 contributed to the relatively large bias and comparability figures given in Table 2.3 for Trial SCNT2. The largest bias and comparability values occurred at the 1/3 path segment, where shears and crosswind reversal problems were most severe. However, wind shears did not affect precision, which remained small for the 1/3 path segment. This is interpreted to mean that the two scintillometers tracked the variability in the wind field consistently, but showed a consistent bias in the magnitude of the measured crosswinds.

The precision values in Table 2.3 show no apparent trend as a function of path position even though the separation between the two optical beams ranged from near zero at the 1/5 path segment to near 0.7 m at the 4/5 path segment. Any effects of this separation on precision are below the measurement threshold. Precision is worst for Trial SCNT2 on 19 November, when there were multiple cross-path wind reversals in light and variable winds. The cross-path wind reversals and decorrelation effects contributed to an approximate doubling of the precision envelope from 0.05 to 0.10 m/s.

Table 2.3. Scintillometer Bias, Comparability, and Precision at Each Path Segment for 255-s Averaged Crosswinds.

Trial	Date	Path Segment 1/5	1/3	1/2	2/3	4/5
			Bias (m/s)			
SCNT2	19 Nov	-.1197	-.3095	-.0039	+.0710	+.1475
SCNT3	20 Nov	-.1079	-.1374	-.0476	+.1418	+.1395
SCNT4	20 Nov	-.1009	-.1635	-.0547	+.1211	+.1185
SCNT5	20 Nov	-.1401	-.1860	-.0201	+.1585	+.1432
SCNT6	21 Nov	-.2207	-.1992	-.0342	+.1179	+.1056
			Comparability (m/s)			
SCNT2	19 Nov	.1587	.3285	.0578	.1276	.1850
SCNT3	20 Nov	.1153	.1434	.0678	.1596	.1583
SCNT4	20 Nov	.1052	.1658	.0669	.1423	.1459
SCNT5	20 Nov	.1464	.1875	.0333	.1756	.1583
SCNT6	21 Nov	.2252	.2008	.0534	.1260	.1199
			Precision (m/s)			
SCNT2	19 Nov	.1042	.1101	.0577	.1060	.1117
SCNT3	20 Nov	.0406	.0412	.0484	.0732	.0747
SCNT4	20 Nov	.0298	.0278	.0386	.0747	.0851
SCNT5	20 Nov	.0426	.0237	.0266	.0754	.0675
SCNT6	21 Nov	.0449	.0248	.0410	.0446	.0566

2.4.4 Time Averaging Effects

Analyses of the crosswind standard deviations and time series were also performed to document the scintillometer's ability to measure the variability in the wind field. Response to variability in the wind field is limited by the instrument's ability to resolve significant turbulence scales. The sonic anemometers served as a useful basis for comparison because their rapid response and short path averaging permit resolution of small turbulence scales. A sonic anemometer sampling rate of 2 Hz, which is too slow for definition of the small but energetic turbulence scales at 2 m above ground level (AGL), was imposed by data collection system limitations. However, because scintillometer line averaging also attenuates the small turbulence scales, there is little to be gained by comparing scintillometer and sonic anemometer standard deviations from data averaged over periods of less than several seconds. Consequently, a 10-s averaging time was selected as an appropriate averaging interval for the standard deviation comparisons.

Figures 2.7 through 2.9 show the effects of averaging time on the standard deviations of sonic anemometer and scintillometer crosswind measurements. The standard deviations in the three figures have been normalized by dividing by the corresponding standard deviations for the 10-s averaged data. As shown by Figures 2.7 through 2.9, the standard deviations of crosswind components decrease monotonically as the data averaging time is increased from 10 s to 255 s. The effects of the tree line on the sonic anemometer turbulence measurements are apparent from comparison of Figures 2.7. and 2.8. During the trial on 19 November (Figure 2.7), winds were generally along the optical path with little perturbation by the trees, and the sonic anemometer standard deviations at all path positions decrease more-or-less in a cluster. The small differences are probably attributable to small-scale terrain effects. During the trial on the afternoon of 20 November (Figure 2.8), westerly winds produced a large crosswind component. The 919- and 830-m sonic anemometer standard deviations for this case decrease in a pattern similar to that shown in Figure 2.7, while the 660- and 600-m standard deviations decrease much more rapidly for the longer averaging times. Attenuation of larger scale (low frequency) eddies at 660 and 600 m due to the blocking effect of the trees is a probable explanation for these results. Similar results are apparent in the corresponding scintillometer data shown in Figure 2.9. The 1/5 path segment, free of wind attenuation through the trees, follows a pattern similar to the 919- and 830-m sonic anemometers. The 1/3 path segment is only partly affected by the tree line, while the lower frequency eddy energy is severely attenuated along the tree-sheltered 1/2, 2/3, and 4/5 path segments. The curves in Figures 2.7 through 2.9 can be represented by an equation of the form

$$y = 100 - B \ln x \qquad (2\text{-}8)$$

where x is the ratio of the averaging interval to the reference averaging interval (10 s) and y is the normalized crosswind standard deviation in percent. For the curves in Figures 2.7 through 2.9, the B term in Equation 2-8 ranges from 5 to 20, increasing as the blockage becomes more pronounced.

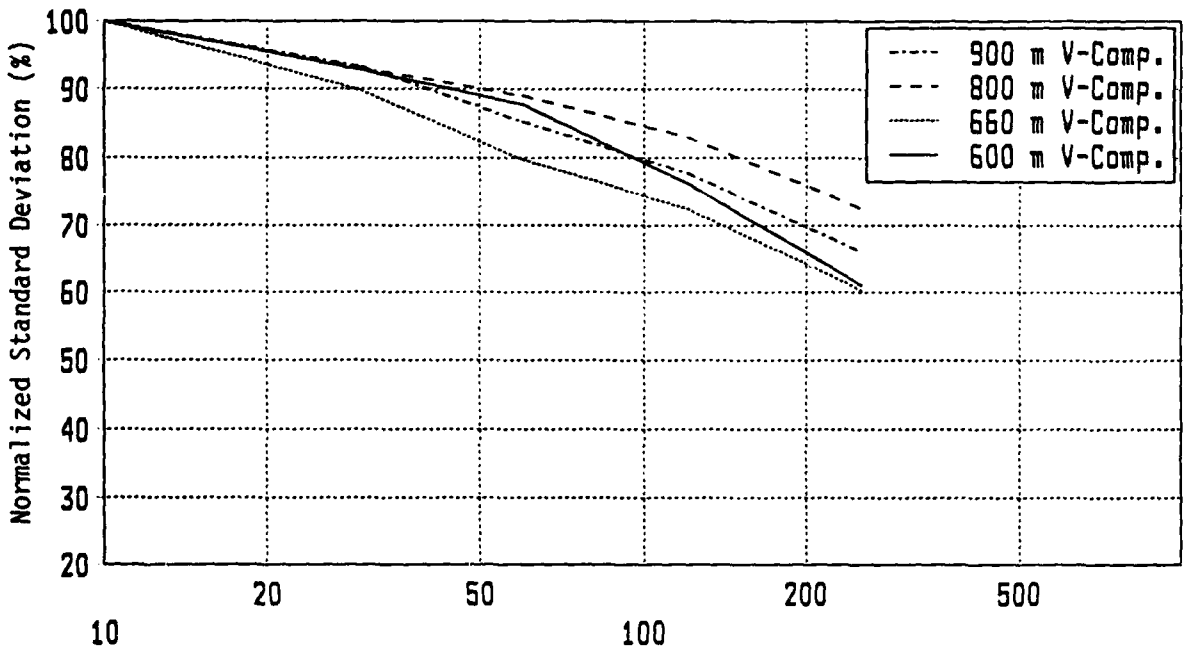

Figure 2.7. Time Averaging Effects on Sonic Anemometer Crosswinds (v-components) for 19 November 1987.

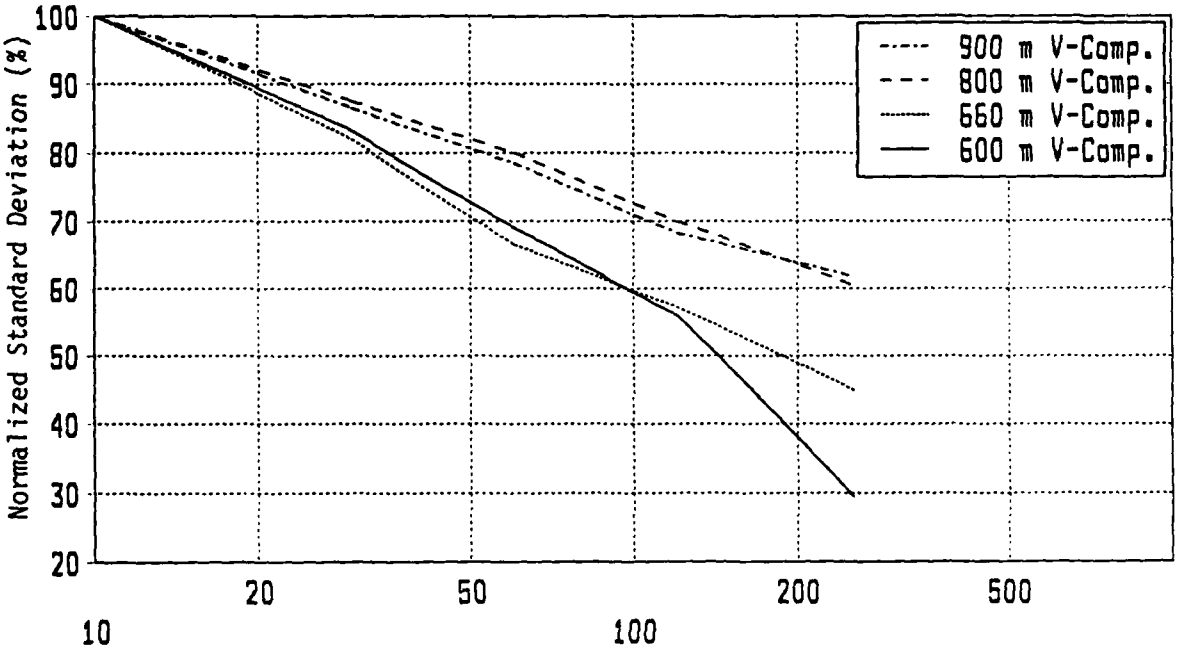

Figure 2.8. Time Averaging Effects on Sonic Anemometer Crosswinds (v-components) for 20 November 1987.

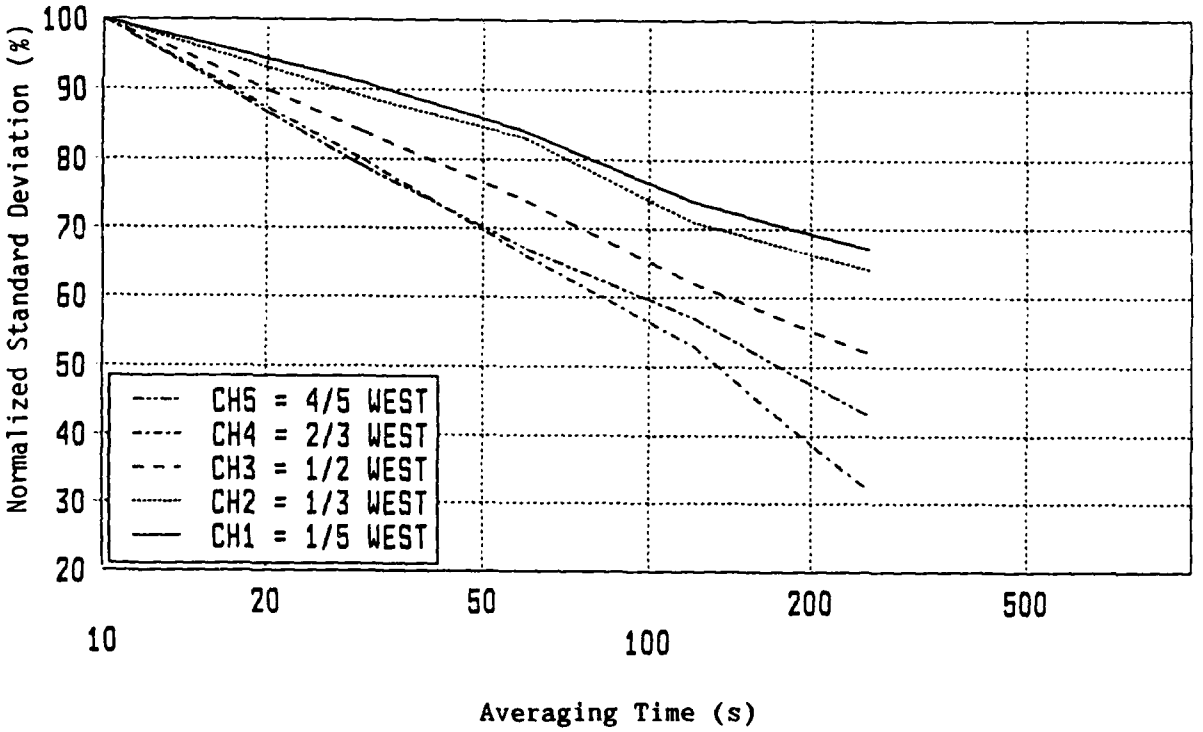

Figure 2.9. Time Averaging Effects on Scintillometer Crosswinds for 20 November 1987.

The consequences of crosswind scintillometer path and time averaging on standard deviation measurements are illustrated on Figure 2.10. Figure 2.10 shows the ratio of the scintillometer crosswind standard deviation for each path segment to the average of the standard deviations obtained from the 919- and 830-m sonic anemometer data. These ratios illustrate a classic tradeoff between path-averaged and point measurements. The path-averaged measurement is more representative of the mean wind, but this enhanced representativeness is obtained at the expense of an attenuated variance, particularly for scales of motion smaller than the path segment length.

Increasing the averaging time can, but does not always, have a similar effect on the crosswind variance as path averaging. The ratio of the scintillometer 1/5 path segment standard deviations to the averaged sonic anemometer standard deviations shown in Figure 2.10 increases as the averaging time increases until this ratio reaches unity (near 120 s). This result illustrates a general equivalence between time and path averaging when the terrain is reasonably homogeneous and turbulence is more-or-less invariant in time. In contrast, the ratios formed using the other path segment standard deviations do not approach equivalence as averaging time increases. This occurs because the tree line removed large scale turbulence elements from the winds passing through these path segments. Therefore, increasing the averaging time to overcome path attenuation effects still leaves a deficit in the scintillometer to sonic anemometer standard deviation ratio.

2.4.5 Scintillometer Performance Problems

The scintillometer does not function properly if a crosswind is absent or if signal strength goes to zero due to interruption of the optical path. No spurious data due to optical path interruptions were detected during the trial series, although signal strength was occasionally interrupted as vehicles driving down the B-1 gun line road passed through the optical path (see Figure 1.2). These brief interruptions registered as a temporary loss of signal strength on the signal strength meter, but time constants in the electronic circuitry apparently prevent temporary interruptions from creating spurious data.

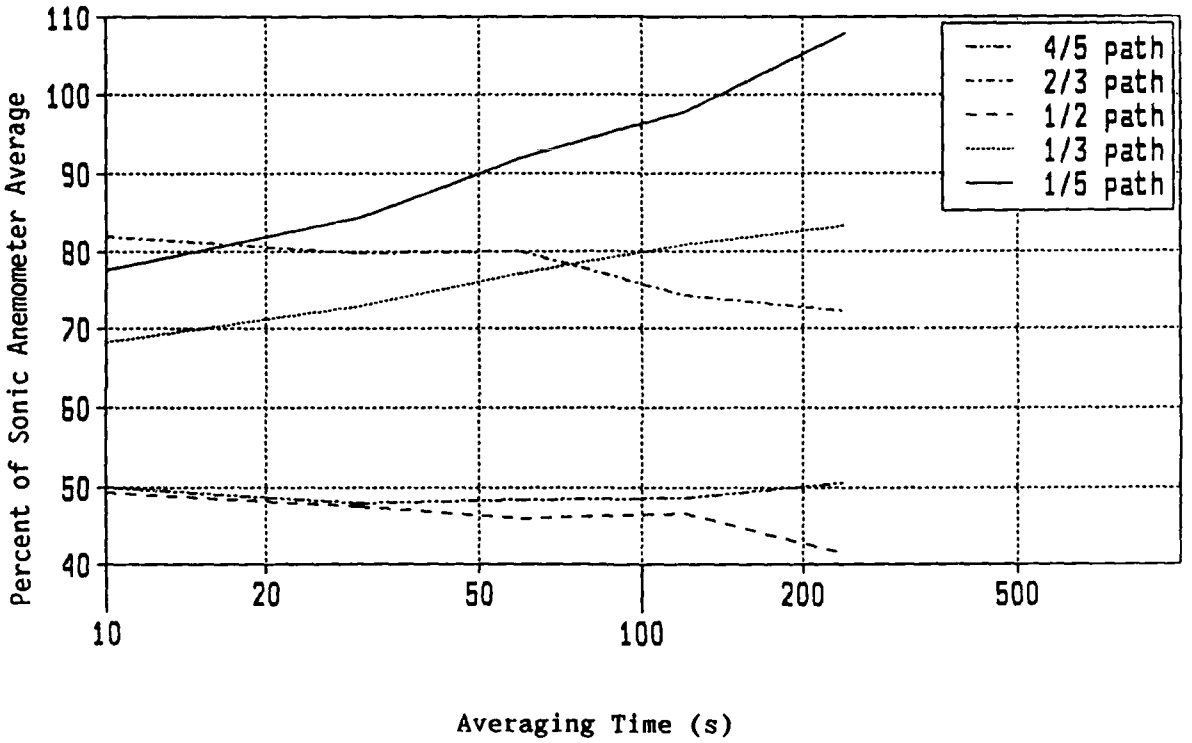

Figure 2.10. Scintillometer/Sonic Anemometer Time Averaging Effects Ratio.

The only significant instrument performance problems occurred on 19 November when the cross-path wind direction was variable. This effect is illustrated in Figures 2.11 and 2.12. Spurious crosswinds, appearing as spikes or as pronounced increases in wind speed, are evident in Figures 2.11(a) and (b) for both scintillometers at the 1/5 path segments, starting at 70 s into the time series. Several smaller spurious readings are also evident later in the time series. The corresponding sonic anemometer measurements (Figures 2.11(c) and (d)) indicate that these spurious readings are associated with very light winds and multiple reversals in the cross-path wind direction. Although the spurious readings shown in Figure 2.11 occurred simultaneously in the data from both scintillometers, Figure 2.12 shows that spurious readings

occurred only in the scintillometer Unit #2 1/3 path segment data. The spurious data are distributed throughout the 19 November data collection period and are associated with multiple cross-path wind reversal conditions. Figures 2.11(c) and (d) and 2.12(c) and (d) show sonic anemometer crosswinds of opposite sign (direction) when the spurious readings occur. The change of crosswind sign within the path segment over which the data are averaged appears to trigger these occurrences. Except for the spurious readings, the path-crossing trends in the crosswind scintillometer crosswinds closely follow the path-crossing trends in the sonic anemometer crosswinds.

The spurious data illustrated in Figures 2.11 and 2.12 are caused by servo lock onto the wrong sign for cross-path wind measurements. The sign of the crosswind is defined by a covariance analysis technique outlined in Section 2.2.4 and described in detail by Ochs et al. (1988). Ochs (personal communication) notes that the time constant on the wind speed integrator is shorter by a factor of 10 than the time constant used with the covariance function that defines the sign of the crosswind. When signal strength is low and the sign of the crosswind is changing rapidly, the servo mechanism used to define sign for crosswind computation is occasionally locked onto the wrong polarity. This causes the wind speed computation to depart from the correct value. The problem is self-correcting once the servos regain lock on the true crosswind sign.

2.4.6 Analyses of the Spectra

Spectra of the scintillometer and sonic anemometer time series data were analyzed to examine the effects of scintillometer line averaging and to identify the frequencies contributing most to the variability in the crosswinds. Cospectra (COS) and quadrature spectra (QUAD) were examined for in-phase and phase-shifted covariances, and statistical analyses were applied to the coherence (COH) data. Background information on spectrum analysis is presented in Appendix B.

The data set used for spectrum analysis was collected on 20 November between 1511 and 1611 EST. The 2 Hz data were averaged into 3-s blocks for the hour to obtain one set of 1200 samples, 1024 of which were used for spectrum analysis. During this period, the winds ranged from 253° to 303° with an average wind direction of 278°, and wind speeds ranged from 1.2 to 3.7 m/s with an average speed of 2.8 m/s. There was no discernible trend in the wind data, and the power in the lowest spectral frequencies usually was an order of magnitude or more below that of the spectral peaks, providing further evidence for only weak trends in the data. The wind speed of 2.8 m/s was used to convert frequencies in hertz to wavelengths in meters, the longest being on the order of 4300 m and the shortest 19 m. Averaging the 2 Hz data to 3-s averages prior to use in the spectrum analysis programs should have minimized aliasing effects. See Koopmans (1974), Jenkins and Watts (1969), or any other comprehensive reference on time series analysis for a discussion of aliasing.

Initial comparisons were made using spectra obtained from measurements along scintillometer path segments. The spectra from path segments 1/5W and 1/5E shown in Figure 2.13 are virtually identical, indicating that the instruments exhibit similar frequency response across all bands. Spectra from other

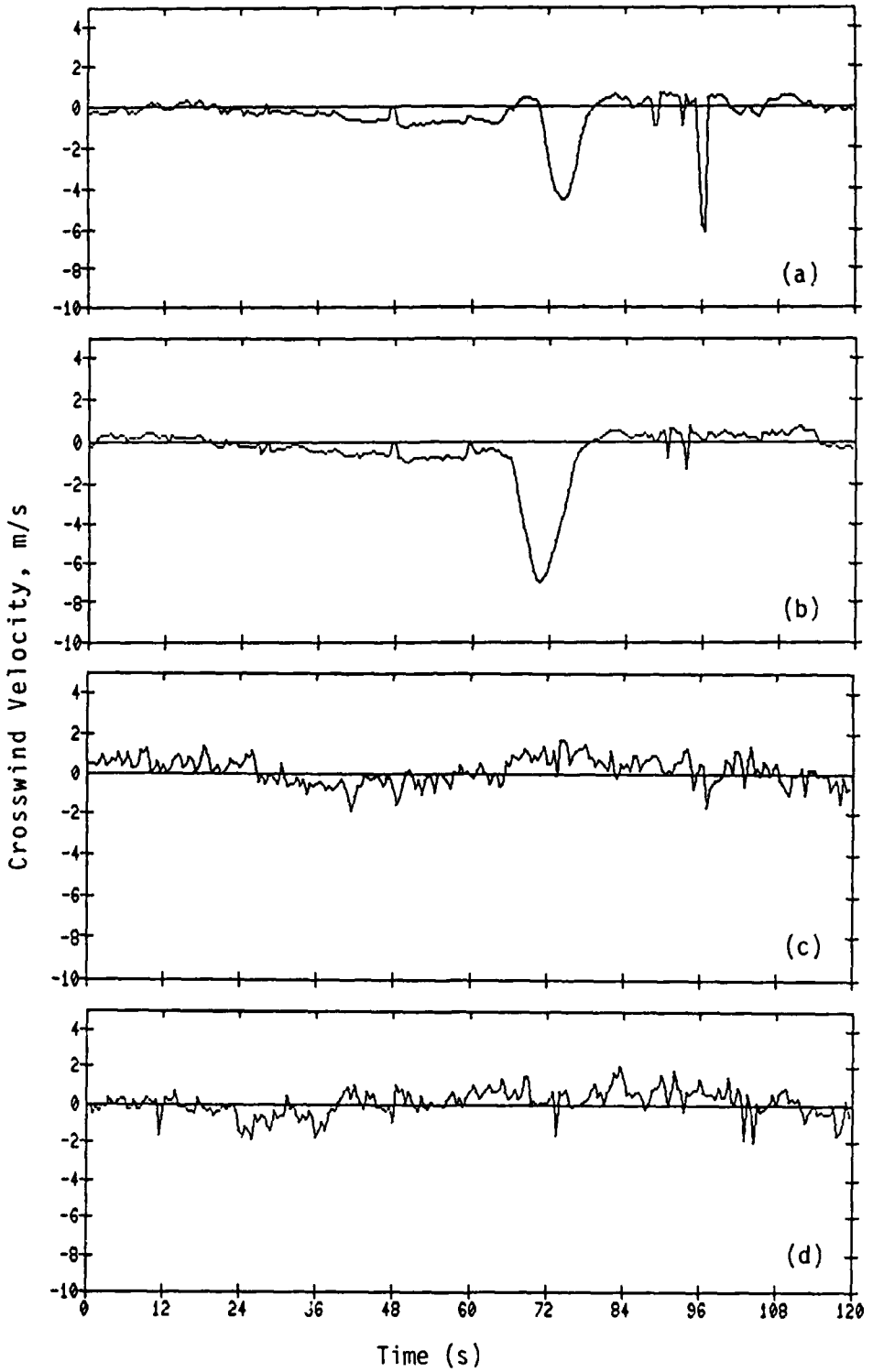

Figure 2.11. Two-Minute Time Series from Crosswind Scintillometer 1/5W (a) and 1/5E (b) Path Segments, and 830 M (c) and 919 m (d) Sonic Anemometer Crosswind Measurements on 19 November 1987, 1426-1428 EST.

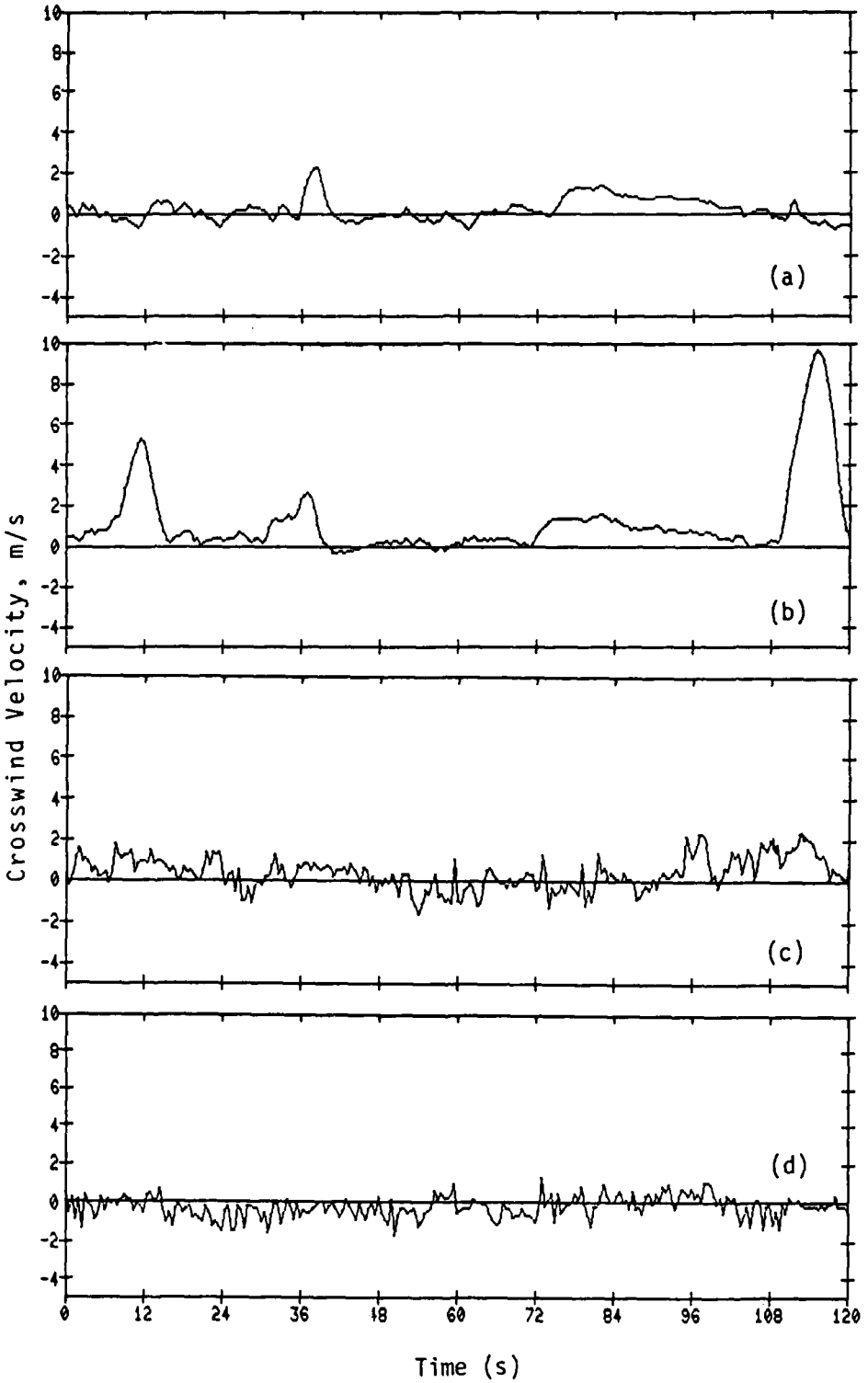

Figure 2.12. Two-Minute Time Series from Crosswind Scintillometer 1/3W (a) and 1/3E (b) Path Segments, and 600 m (c) and 660 m (d) Sonic Anemometer Crosswind Measurements on 19 November 1987, 1335:16 to 1337:16 EST.

parallel path segments exhibited similar agreement, demonstrating consistent frequency response along the entire optical path. The minor differences in spectrum detail are likely due to the slight differences in instrument performance that caused the bias reported in Section 2.4.3.

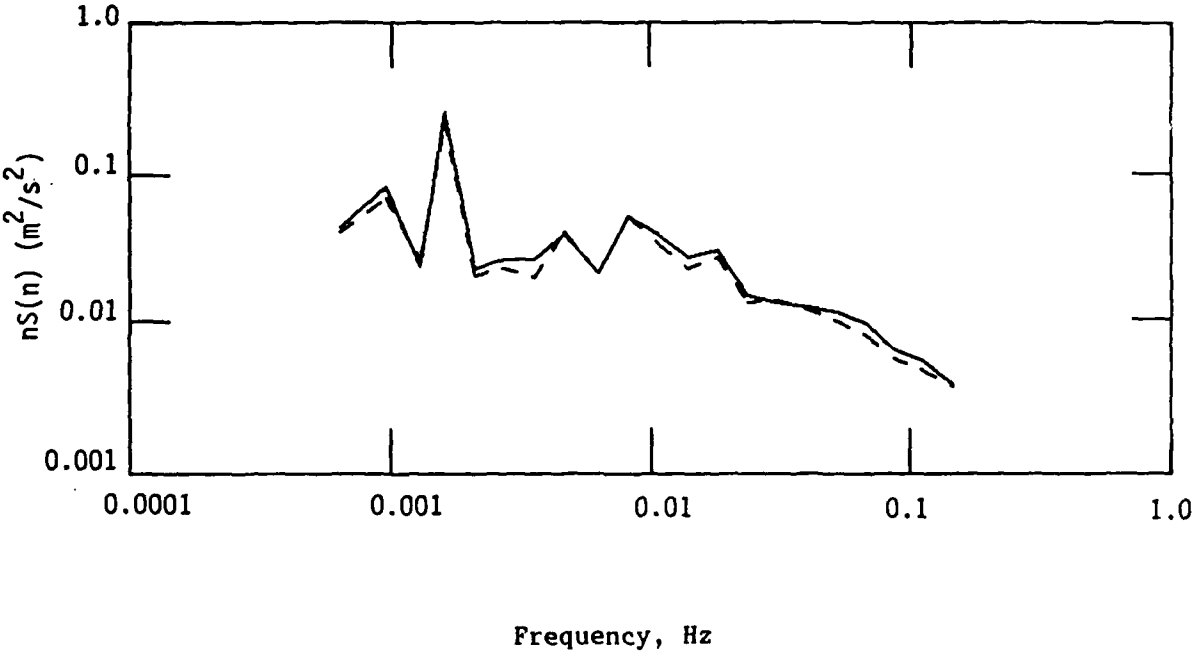

Figure 2.13. Spectra from the 1/5 West (——) and 1/5 East (----) Crosswind Scintillometer Path Segments.

The dominant spectrum feature in Figure 2.13 is the peak near 0.0016 Hz. The dominant spectrum peak has a wavelength near 1700 m and a period on the order of 10 min. A similar peak, somewhat reduced in magnitude, was found in the 1/3 path segment spectra, but these peaks did not appear in spectra from path segments farther down the optical path. Spectral maxima occurred at or near this frequency on the 919- and 830-m sonic anemometer spectra as well, although the sonic anemometer spectral energy was somewhat more broadly distributed. These spectral maxima identify the time scales of the most energetic crosswind gusts. Therefore, the dominant turbulent component in the wind field for the open terrain near the 1/5 scintillometer path segment occurred as gusts with periods on the order of 10 min. This is consistent with the reported pre-frontal weather characterized by variable cloudiness and intermittent convective rainshowers.

A much different wind gust energy distribution pattern is evident in the crosswind spectra obtained from scintillometer path segments sheltered by the tree line. Figure 2.14 shows spectra from the 1/5 west and 4/5 east crosswind scintillometer path segments. The 4/5W path segment spectrum has a power minimum at the lower frequencies and a broad maximum between 0.01 and 0.1 Hz. The tree line has removed wind energy from gusts with periods on the order of 10 min and converted it to gusts with periods of 10 to 100 s. Therefore, the tree line has not only caused a crosswind-speed shear, as discussed in Section 2.4.2, but has also caused a "shear" in turbulence scale.

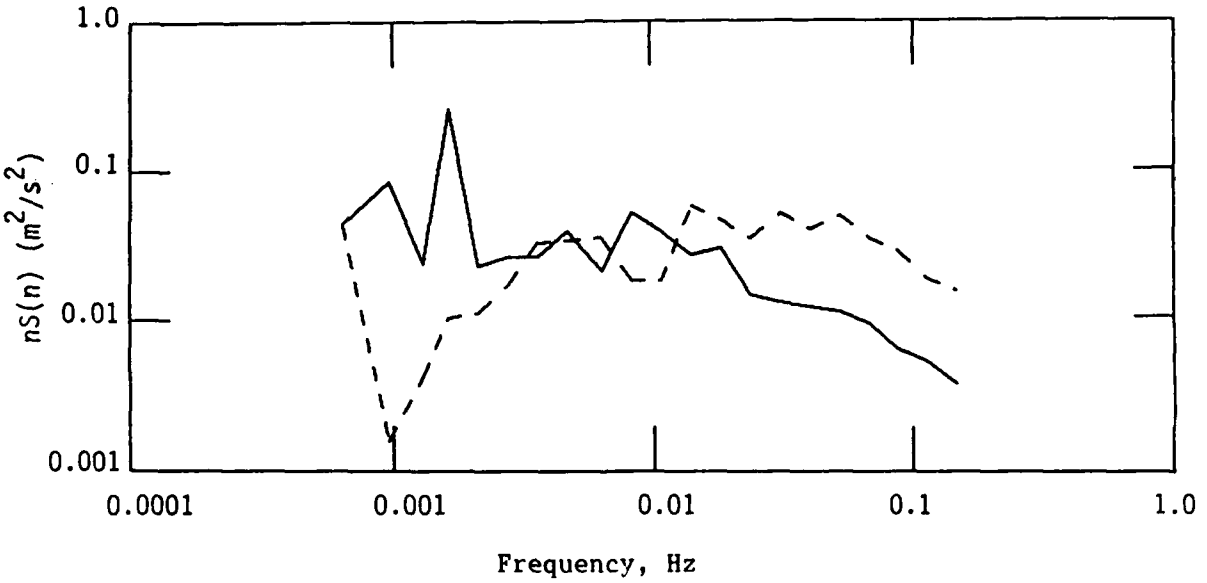

Figure 2.14. Spectra from the 1/5 West (——) and 4/5 West (----) Crosswind Scintillometer Path Segments.

The transfer of energy from lower to higher frequencies along the optical path can be analyzed in more detail using the cospectra and quadrature spectra. The 1/5W versus 1/5E COS in Figure 2.15 shows a strong positive maximum, with only a slight hint of a positive QUAD maximum at the dominant 0.0016 Hz frequency. Therefore, the dominant harmonics are strongly in phase, as would be expected along nearly identical paths. COS and QUAD magnitudes remain small at the higher frequencies for two reasons. First, because turbulent eddies tend to be uncorrelated at higher frequencies, the covariances represented by COS and QUAD are correspondingly small. Second, because line-averaging attenuation effects (evaluated later in this section) increase with increasing frequency, the magnitudes of the covariances are

further reduced. The 1/5W versus 1/5E COS, QUAD, PHASE, and COH serve as reference values for the analysis to follow.

In interpreting Figures 2.15 through 2.19, it should be remembered that cospectra and quadrature spectra are products of the in-phase and 1/4 wavelength phase-shifted harmonics from two spectra. These products produce frequency-dependent covariances that are positive or negative, depending on whether the harmonics are in phase or 180° out of phase. Like any covariance, COS and QUAD are not normalized quantities. Therefore, the absolute magnitudes of COS and QUAD obtained from separate spectra should not be directly compared. However, COS and QUAD in this analysis are all obtained with reference to a common spectrum, the 1/5W scintillometer path segment spectrum. Therefore, the magnitudes of COS and QUAD for Figures 2.15 through 2.19 are scaled in relative units for the purpose of intercomparison with each other.

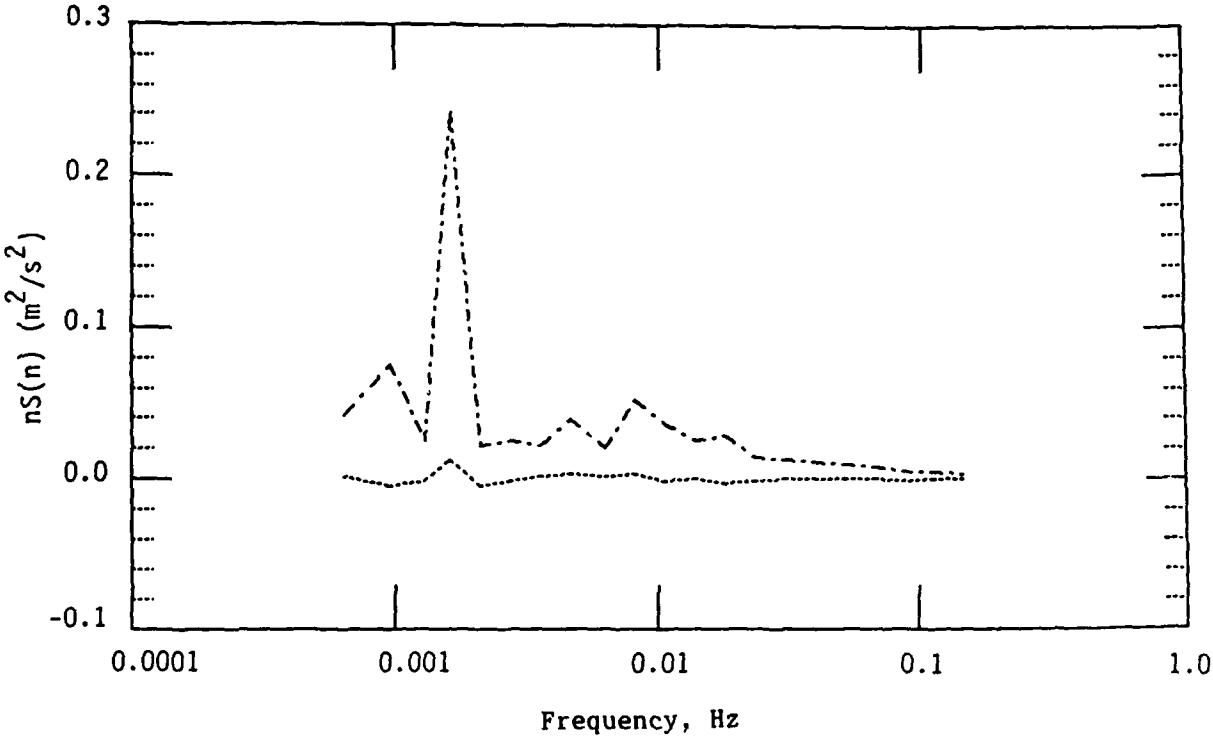

Figure 2.15. Cospectra (-·-·-) and Quadrature Spectra (----) for Crosswind Scintillometer Path Segments 1/5W and 1/5E.

Three things happen to eddies as they translate from one point or path segment to another: The phase angles shift, amplitudes decay, and patterns become decorrelated. Phase shift is a consequence of eddies translating through the fixed frame of reference used for measurement. An eddy carried by the wind past one measurement position at time t will arrive at a downwind position at $t + \Delta t$. Translation changes the signs and magnitudes of COS and

QUAD, but their absolute amplitude (COS^2 + $QUAD^2$) remains unchanged so long as there is no gain or loss of energy. During pure translation, PHASE changes with COS and QUAD, but COH remains at unity. Amplitude decays as energy is removed from the eddies. This energy loss decreases (COS^2 + $QUAD^2$) in proportion to the loss of power in the spectra, but does not change PHASE or COH. Eddy patterns become decorrelated with the injection of energy as new eddies form. Energy injection occurs in random patterns, which decreases (COS^2 + $QUAD^2$) even though there is a net gain in spectral power. This effect introduces unpredictable PHASE angles, and decreases COH.

The COS, QUAD, PHASE and COH between the 1/5W path segment spectrum and spectra from path segments progressively farther down the optical path, as shown on Figures 2.16 through 2.19, illustrate translation, and amplitude decay in the lower spectral frequency bands, and decorrelation effects in the higher bands. The 1/5W versus 1/3W COS shown in Figure 2.16 exhibits the prominent spectral maximum at 0.0016 Hz, but its amplitude is reduced to 55% of the corresponding value for the reference 1/5W vs 1/5E COS (Figure 2.15). COH remains at 1.0, indicating no decorrelation effects at this frequency. The development of a negative QUAD peak at 0.0016 Hz indicates a shift in phase due to translation. Non-zero QUAD components also appear between 0.003 and 0.005 Hz. In contrast, decorrelation effects at frequencies above 0.01 Hz sharply decreased amplitudes, introduced random phase angles, and decreased coherence at these frequencies.

The COS and QUAD for the 1/5W path segment versus the 1/2W path segment (Figure 2.17) show a further decrease in COS and an increase in the magnitude of negative QUAD. Amplitude decay reduced (COS^2 + $QUAD^2$) to 42% of its reference value. Also, a secondary positive QUAD component appears centered near 0.006 Hz. This secondary component evolves into a positive COS component at a frequency near 0.008 Hz for the 2/3W path segment, as illustrated on Figure 2.18. The (COS^2 + $QUAD^2$) at 0.0016 Hz for the 2/3 path segment has decreased in magnitude to 1 percent of its reference value. The spectral peak formerly found at 0.0016 Hz is overshadowed by a peak near 0.001 Hz for the 2/3 path segment. Spectral intercomparisons of the 1/5W and 4/5W path segment crosswinds (Figure 2.19) reveal minor negative COS and QUAD peaks near 0.0016 Hz, and a secondary COS peak near 0.003 Hz.

The foregoing analysis reveals information on how eddies of various frequencies interacted with the tree line. The high frequency end of the spectrum decorrelated between adjacent path segments. This is consistent with the observation that patterns of small eddies evolve rapidly and are less likely to translate intact between path segments than larger eddies. Also, the physical size of these small eddy patterns make them less likely to pass both path segments. A further consideration is that energy tends to be partitioned randomly during eddy decay. Therefore, eddy energy transferred by the tree line from the larger to smaller eddies is randomly distributed. In contrast, the larger eddies exhibited a gradual shift in phase and decrease in amplitude due to tree line effects, but retained their coherence because there was no eddy energy added at these frequencies. Eddy scales in the intermediate 0.003 to 0.01 Hz range exhibited occasional spectral correlations with the reference path segment. Figure 2.14 shows that these eddies did not gain or

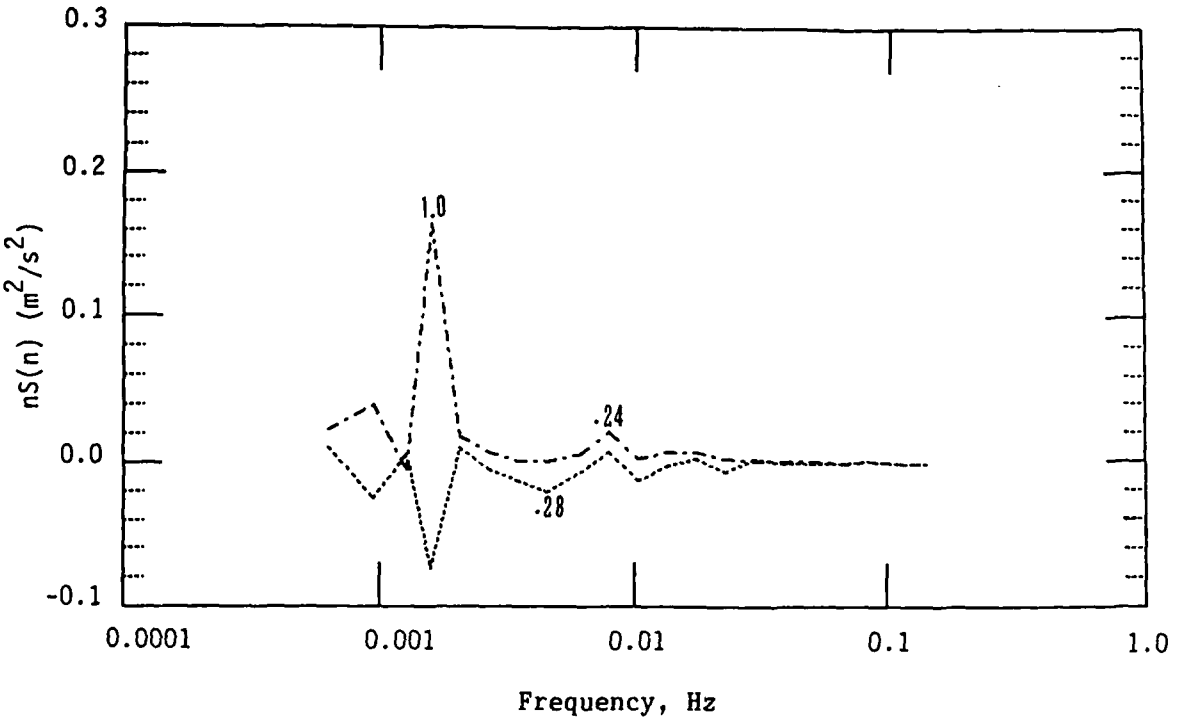

Figure 2.16. Cospectra (-·-·-) and Quadrature Spectra (-----) for Crosswind Scintillometer Path Segments 1/5W and 1/3W.

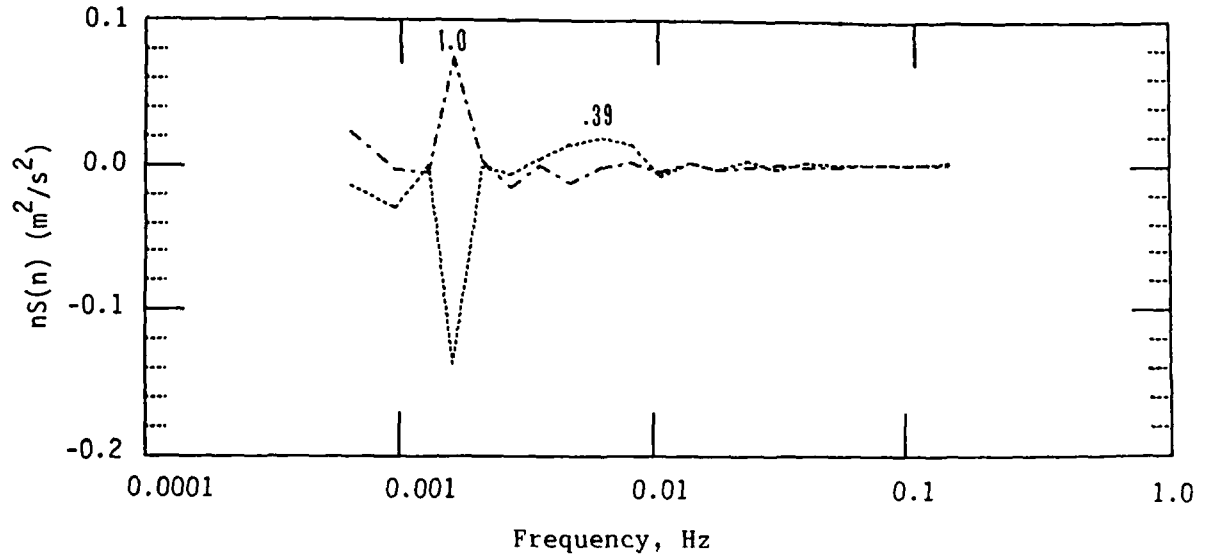

Figure 2.17. Cospectra (-·-·-) and Quadrature Spectra (-----) for Crosswind Scintillometer Path Segments 1/5W and 1/2W.

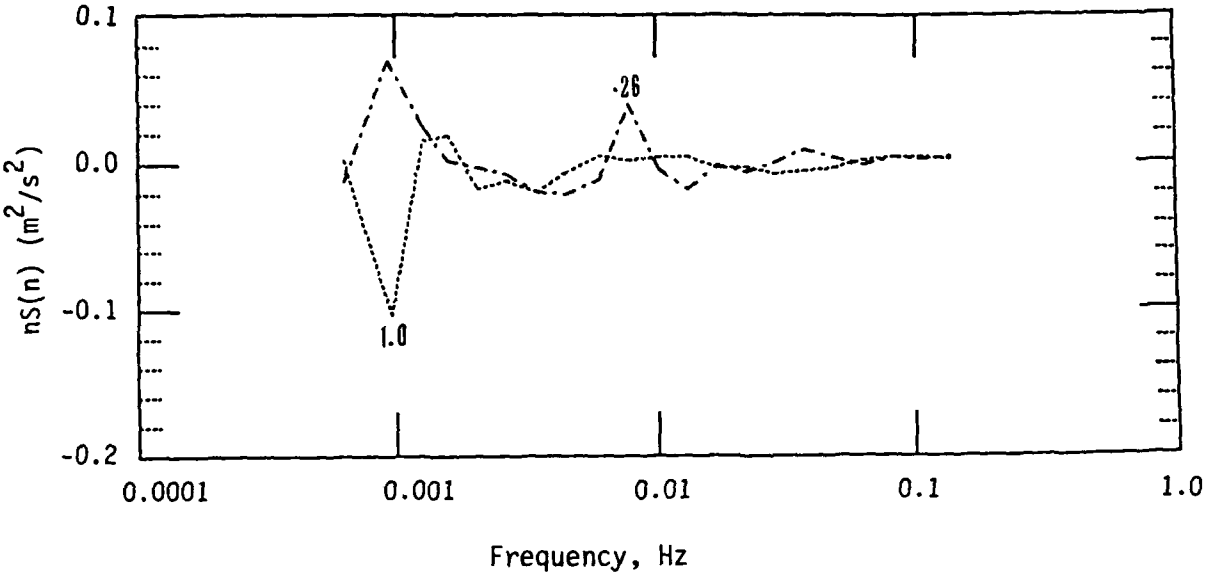

Figure 2.18. Cospectra (—·—·—) and Quadrature Spectra (-----) for Crosswind Scintillometer Path Segments 1/5W and 2/3W.

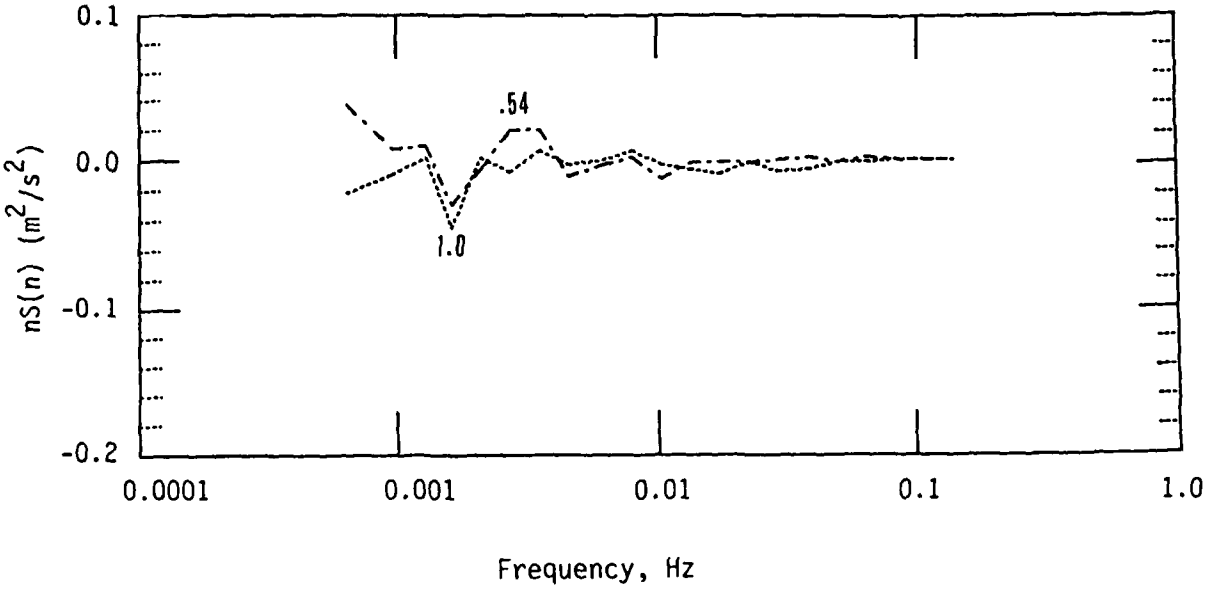

Figure 2.19. Cospectra (—·—·—) and Quadrature Spectra (-----) for Crosswind Scintillometer Path Segments 1/5W and 4/5W.

lose energy as a result of interaction with the tree line, and therefore suffered less amplitude reduction and decorrelation effects than exhibited at the higher and lower frequencies.

An obvious question arises concerning the statistical significance of information found in Figures 2.15 through 2.19. Koopmans (1974) offers a technique to evaluate the statistical significance of the coherence of these features. The null hypothesis for the significance test is that COH does not differ significantly from zero, while the alternative hypothesis is that a significant non-zero COH exists. For a sample size of 1024 and a lag of 22, as used to produce these spectra, Koopmans' Tables A9.1 and A9.2 require COH to exceed 0.375 for 90 percent confidence that COH is nonzero, and to exceed 0.325 for 80 percent confidence that COH is nonzero. COH values are printed above COS and QUAD peaks of Figures 2.15 through 2.19. The major peaks at 0.0016 Hz remain statistically significant for Figures 2.15 through 2.19 in spite of the decline in amplitude and shift in phase. Although the tree line attenuates the amplitude and shifts the phase of the low frequency gust components, it does not destroy the correlation between these components. The significance of correlations at the intermediate frequencies are less certain.

The gross effects of path averaging on the crosswind variance were presented in Section 2.4.4. Details of the power attenuation at the higher spectral frequencies are illustrated in Figure 2.20 by comparison of the 1/5W path segment spectrum with the 830-m sonic anemometer v-component spectrum. The sonic anemometer spectrum is relatively flat across the range of frequencies, while the scintillometer spectrum shows a steady decrease in power as frequency increases, particularly for frequencies greater than .01 Hz. This occurs because the 15-cm sonic anemometer path averaging is two orders of magnitude smaller than the 19-m path length associated with the highest spectral frequency, while the scintillometer's 100-m path averaging is considerably larger than the path lengths associated with the higher spectral frequencies.

Silverman (1968) derived a spectrum transfer function that describes the effects of path averaging on measurement as a function of the ratio of the path averaging length (α) to harmonic wavelength (ω). This transfer function asymptotically approaches 1.0 as α/ω becomes small and zero as α/ω becomes large. Because the sonic anemometer's α/ω is small, its spectrum transfer function is essentially 1.0 for the entire spectral frequency range used in this study. Therefore, the ratio of power in each scintillometer spectral harmonic to the corresponding power in each harmonic of representative sonic anemometer spectra can be used with this transfer function to compare scintillometer path attenuation effects with Silverman's theoretical curve.

The comparison with Silverman's curve was done using a ratio of the averaged power from the 1/3W and 1/3E scintillometer crosswind spectra to the averaged power from the 600- and 660-m sonic anemometer crosswind spectra. These averaged power ratios are plotted versus frequency in Figure 2.21 along with the spectrum transfer function from Table 1 of Silverman (1968). Because the mean wind direction for this data period was at a 62° angle with the

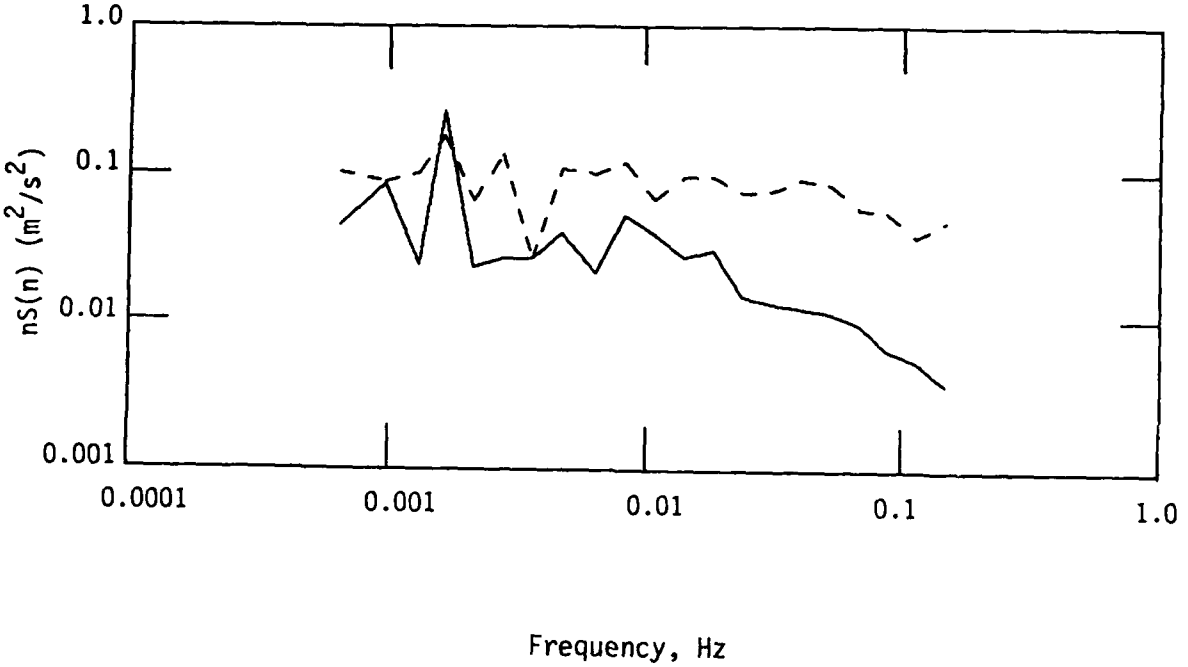

Figure 2.20. Spectra from the 1/5W Crosswind Scintillometer Path Segment (———) and the 830-m Sonic Anemometer v-Component Crosswind (-----).

optical path, the transfer function for a 60° angle of attack was used. The points on Figure 2.21 representing scintillometer/sonic anemometer power ratios exhibit considerable scatter, but follow the general trend of the transfer function curve. Three-point smoothing was subsequently applied to these points, and the resulting smoothed plot tends to conform to the transfer function curve at the higher frequencies.

The differences shown in Figure 2.20 between the scintillometer and sonic anemometer spectra at low frequencies are not explained by path averaging effects. These differences appear as a major peak in the scintillometer power at 0.0016 Hz (Figure 2.20), while the sonic anemometer power is more broadly distributed. These differences are partly explained by: (1) the small number of block estimates used to compute power at the lower frequencies, and (2) the inadequacy of the representation of path-averaged winds by point wind measurements made using only two sonic anemometers. However, these factors do not fully explain the consistently low scintillometer power ratios at low α/ω ratios as seen in Figure 2.21.

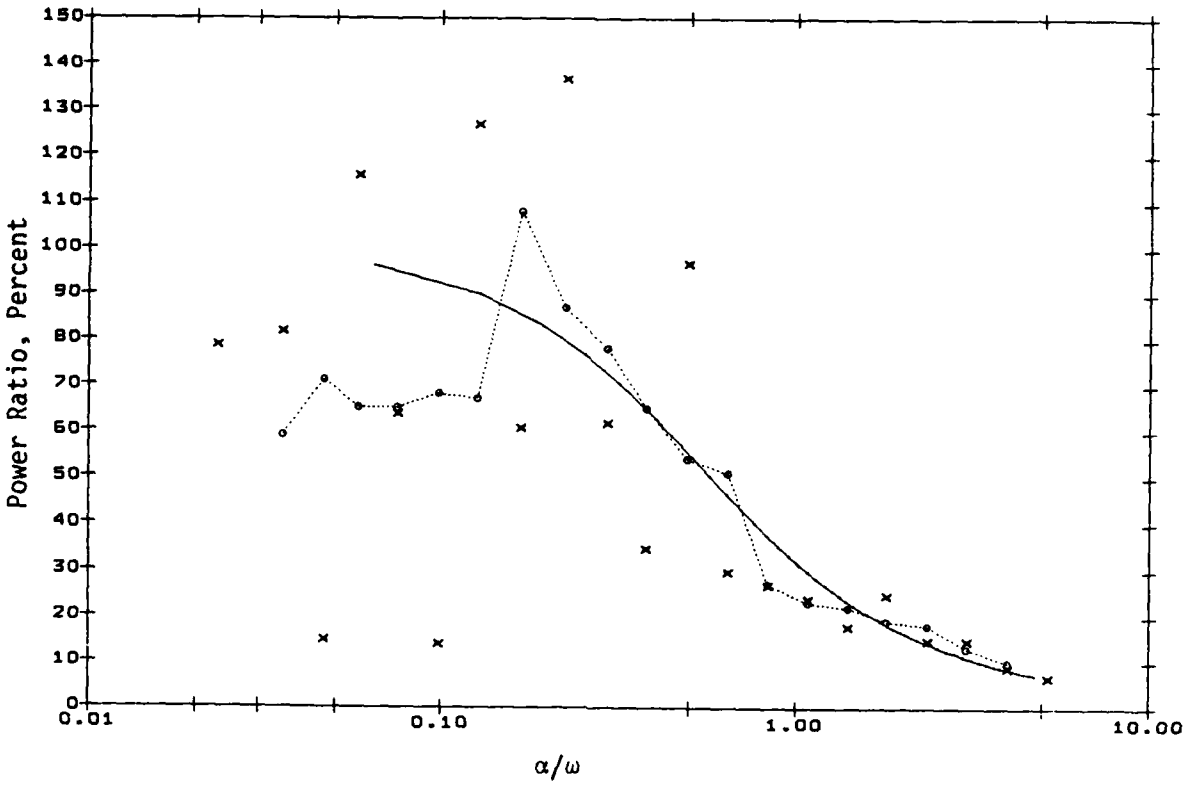

Figure 2.21. Ratios of the Scintillometer to Sonic Anemometer Power by Frequency Band (x) Versus the Path Length to Wavelength Ratio (α/ω), the Power Ratios After 3-Point Smoothing (---0---), and the Silverman (1968) Transfer Function (———).

2.5 ANALYSIS SUMMARY

2.5.1 Equipment Setup and Operation

A field instrument should be reasonably robust, convenient to move, and easy to set up. The instrument should come with quick, convenient procedures to check operational status, and should retain alignment and calibration once it is operational. Instrument output should be in an appropriate and accessable format that is easily monitored, both visually and electronically. The prototype crosswind scintillometer met all of these conditions during this test.

The crosswind scintillometers were shipped from the Colorado ERL/WPL offices to APG in unpadded wooden crates. The metal bars holding detector assembly circuit boards in one receiver unit were bent when the unit was unpacked, indicating that it had been dropped or severely jarred during shipment. The bent bars were straightened, and the unit was operational after reassembly. Survival of rough handling during shipment indicates that the crosswind scintillometer is robust and would likely withstand field handling conditions.

Crosswind scintillometer setup procedures are simple and straightforward. The transmitter was placed on a stack of concrete blocks, and the receivers were placed in the rear of a 2 1/2-ton truck. The concrete blocks and truck suspension provided sufficiently vibration-free platforms for operation. Neither movement in and around the truck nor the shock and blast from a nearby tank gun adversely affected scintillometer alignment and operation. The transmitters and receivers came equipped with sunshades, but the low sun angles during the November tests required additional measures to shade the receivers during the afternoon hours. The sun azimuth and elevation angles relative to the optical path remain a critical operational consideration because direct sunlight on the large-aperture lenses rapidly generates high temperatures that burn out the equipment. Attention to this detail is required when the sun angle is within 15° of the optical path.

The crosswind scintillometer is easily calibrated and operated. A calibration switch provides the means for a quick check of the scintillometer receiver electronic circuit status. Because the transmitter is simply a continuously active signal source, its operational status is apparent from the signal strength meter readings. Instrument output can be visually monitored using the five crosswind meters on the rear panel of each receiver. Analog outputs are available on adjacent connectors. The wind measurement readouts for the five path segments also permit real-time inter-path consistency checks of the crosswind measurements. Optical alignment is easily established using the rifle scopes mounted on the transmitter and receiver housings, and fine adjustments are made until the signal strength meter shows its maximum value. An important operational requirement is that all brush, branches, etc. be removed from the vicinity of the optical path because the movement of small objects through the optical path can cause erroneous, scintillation-like readings. On the other hand, temporary interruption of the optical path by large objects such as vehicles moving along the B-1 service road caused only temporary decreases in signal strength and produced no spurious data.

2.5.2 Operation In Adverse Conditions

The optical scintillometers were used under adverse conditions to assess their operational limitations. Adverse conditions for a scintillometer include very high or very low C_N^2 values, reduced visibility due to fog or precipitation, and wind reversals across the optical path. Testing under high C_N^2 conditions was not possible during the November APG trials. However, Ochs (personal communication) attempted to operate the crosswind scintillometer over a 2.6-km path in high C_N^2 conditions, but found the signal-to-noise (SNR) ratio too low for usable data. Operation over a 1-km path during the APG tests with low to moderate C_N^2 produced a strong SNR. Several periods of light precipitation were encountered during the APG trials. These produced no noticeable effect on the SNR for visibilities as low as 2 km in snow. Further reductions in visibility would eventually have an effect on scintillometer performance, but there was no opportunity to test the limits during the APG trials.

Wind reversals across the optical path created the only significant operational problems during the APG trials. Difficulties occur when there are multiple crosswind reversals occurring simultaneously within the optical path.

During these conditions, the servo that defines the crosswind sign may get out of phase with the actual crosswind sign. The wrong polarity is then used for crosswind computation, and an erroneous wind speed spike occurs in the crosswind output. This condition is self-correcting once the correct polarity is re-established. This wind reversal polarity problem was brought to the attention of the instrument designer Gerard Ochs. He believes that an adjustment of servo time constants so that the crosswind polarity and speed computation circuits stay more in-phase is likely to minimize this problem. These crosswind reversal episodes occur during light and variable along-path winds, which are of minimal interest for ballistics testing.

2.5.3 Measurement Performance

The scintillometers performed without failure during the entire test and provided crosswind measurements comparable to the measurements obtained from the fixed-site wind instruments. A number of techniques were used to assess measurement performance. Mean crosswind speeds computed from GMQ-11 aerovanes, sonic anemometers, and scintillometers were compared, and standard deviations of the crosswind components from the scintillometers and sonic anemometers were also compared. Spectrum analysis techniques were also used on scintillometer and sonic anemometer data to determine performance as a function of frequency.

Mean crosswind intercomparisons with GMQ-11 aerovanes and sonic anemometers illustrate some of the difficulties inherent in trying to compare fixed-point measurements to path-averaged measurements, especially in inhomogeneous terrain. Scintillometer mean crosswind measurements appear to be biased toward lower speeds than the corresponding GMQ-11 or sonic anemometer crosswinds. The scintillometer calibration factor K, which adjusts for medium decorrelation effects, is probably responsible for a 5 percent uncertainty in scintillometer crosswind measurements.

A detailed intercomparison was made of scintillometer crosswind measurements on adjacent optical paths formed by one transmitter and two closely spaced receivers. Instrument performance was described using the standard measures of bias, comparability, and precision. A systematic measurement bias attributable to instrument differences was found. Scintillometer Unit #2 consistently measured stronger crosswinds towards the transmitter end of the optical path, while Unit #3 measured stronger crosswinds towards the receiver end of the optical path. The average comparability of 14 cm/s and precision of 5 cm/s are well within the performance range achieved by modern high quality wind monitoring equipment.

An analysis of standard deviations obtained from the sonic anemometer and scintillometer data averaged over progressively larger time intervals provided a quantitative description of the removal of low frequency turbulence from the wind by the tree line. Scintillometer path averaging also attenuated standard deviations for the shorter averaging times. This indicates that the scintillometer has limited application for mechanical turbulence measurements, although it does measure the gross crosswind gustiness.

Power spectrum analysis was used to define the frequency-dependent gustiness in wind measurements along the B-1 anemometer line. Spectra from cross-

wind scintillometer Unit #3 are virtually identical to the corresponding spectra from Unit #2, differing only slightly in the magnitudes of the spectral peaks. These minor differences in detail are likely due to slight inter-instrument bias. The correspondence in spectra indicates that scintillometer Units #2 and #3 are performing in a virtually identical fashion over the range of sampling frequencies.

Intercomparisons of spectra from different segments along the optical path reveal details of how the winds interacted with the tree line. Comparison of the open-fetch 1/5 path segment spectrum with the spectrum from the tree-sheltered 4/5 path segment shows a shift in power spectral peaks from lower to higher frequencies due to the removal of energy from larger scale eddies by the tree line. Spectrum analysis reveals that the tree line creates a shear in both crosswind speed and turbulence scale. Cospectra and quadrature spectra illustrate low frequency phase delay and amplitude loss and high frequency decorrelation in the turbulent wind field due to the tree line.

The effects of path averaging on the crosswind scintillometer spectra were investigated using the Silverman (1968) algorithm. Averaged sonic anemometer spectra were used to approximate point measurements because of the comparatively short sonic anemometer path averaging. Smoothed ratios of the scintillometer spectra to the sonic anemometer spectra approximate the Silverman curve at the higher frequencies, indicating that the gradual decrease in scintillometer spectral power at these frequencies is an attenuation due to path averaging. These results also suggest a method for adjusting the scintillometer spectra for path averaging effects, although the uncertainty of this adjustment technique is likely to increase with the degree of attenuation.

Unexplained differences were found between the sonic anemometer and scintillometer responses at the low frequency end of the spectra. A major spectral peak at 0.0016-Hz occurred in the scintillometer spectra taken near the transmitter end of the path, with progressive diminution of this peak at path segments closer to the receiver. The 0.0016-Hz peak cannot be solely an artifact of scintillometer performance. The sonic anemometer low frequency spectral power was more broadly distributed. These differences in the spectra are not readily explainable.

2.6 CONCLUSIONS

The field test of the prototype crosswind scintillometer demonstrated that this instrument has significant potential for field applications where multiple path-averaged wind measurements are needed. The instrument's remote sensing capability also offers the opportunity to obtain wind measurements without the need to position sensors at the measurement location. Applications may include crosswind measurements in rough terrain, across a gorge, along a runway, or along an artillery range line of fire. The scintillometer design is sufficiently robust for field use, and the equipment is easily set up, aligned, and operated. The most significant constraints on field applications are:

(a) The transmitter and receiver must be mounted on stable, vibration-free platforms.

(b) Brush and other objects must be removed from the optical path.

(c) Direct sunshine must not fall on the optics.

The operational range for the prototype crosswind scintillometer is on the order of 1 km, with five wind measurement segments evenly distributed along the optical path. However, the spatially-averaged filter technique can be adapted for different path lengths or combinations of path segments by selecting appropriate combinations of filter sizes and operating frequencies. This technique could, therefore, be optimized for crosswind measurement on an artillery range.

The crosswind scintillometer is capable of providing more representative crosswinds along a ballistic path than is possible using any reasonable number of fixed-point wind sensors. Scintillometer path averaging reduces considerably the statistical uncertainty inherent in crosswind measurement. However, the advantage gained in defining the mean crosswind is lost in defining the crosswind variance because path averaging attenuates higher frequency turbulent motions. This attenuation can be partly compensated using a transfer function, but the scintillometer's 1-s data rate limits its application to the measurement of lower frequency turbulent motions. These lower frequency turbulent motions, or gusts, cause wind loading on projectiles and should be accounted for in ballistics performance tests. The crosswind scintillometer is well suited for this measurement application.

Problems encountered during the crosswind scintillometer field test included uncertainties in the calibration factor and spurious wind readings during wind reversals across the optical path. The calibration factor, which compensates for medium decorrelation along the optical path, is likely to vary as a function of wind angle. Additional field trials are needed to better define this calibration factor. Spurious wind readings can be minimized by adjusting electronic circuit delay so that cross-path speed computations are performed using the appropriate crosswind sign. Neither problem is serious and both are amenable to solution with further crosswind scintillometer development and testing.

SECTION 3. APPENDICES

APPENDIX A: A DESCRIPTION OF SCINTILLOMETER OPERATION

Scintillometer operation is based on certain assumptions about atmospheric turbulence. Consequently, scintillometer performance is dependent on how well the atmosphere conforms to these assumptions. The atmosphere is continuously adjusting to the flux of heat by turbulent mixing, which creates a spectrum of turbulent elements (eddies) of varying densities. Density discontinuities between eddies cause changes in the atmospheric refractive index. A model of turbulence initially proposed by Kolmogorov is applied to the refractive index power spectrum. The model depicts a refractive-index spectral density proportional to C_N^2, representing the strength of refractive index fluctuations. Tatarskii (1961) defines C_N^2 as a function of differences in the index of refraction (N) at scalar separation distances (r) by

$$C_N^2 = \overline{(N(x) - N(x+r))}/r^{2/3} \qquad \text{(A-1)}$$

where the overbar indicates a time-averaged quantity.

The Kolmogorov model is assumed to represent turbulence in the inertial subrange, a range of eddy sizes from a few millimeters to several tens of meters. In this model, turbulent energy is injected at the larger eddy sizes (the outer scale) and is transferred to smaller scales as the larger eddies break up. Energy is transferred to progressively smaller scales essentially without loss until the smallest scale (inner scale) is reached. Beyond the inner scale, turbulent energy is converted to heat through viscous dissipation. The real atmosphere seldom exhibits the ideal turbulent state presented in this model, which assumes the existence of steady-state uniform turbulence. Also, density discontinuities may be very weak in near-neutral conditions. These factors constrain the precision and range of measurements made by wave propagation techniques.

Scintillometer crosswind measurements are based on the "frozen turbulence" hypothesis proposed by Taylor (1938) which states that, over appropriately small periods of time, turbulence elements are carried along by the wind without significant decay. Time-lagged correlation techniques are used to match scintillation signatures of eddies translating from one optical path to a parallel path. The highest correlation is assumed to occur at a time lag equal to the time taken for eddies to translate from one path to the other. The path separation distance divided by the time lag of the highest correlation defines the cross-path wind speed. The frozen turbulence hypothesis breaks down for extended path separation distances and for some atmospheric conditions. The breakdown of this hypothesis is called medium decorrelation. Medium decorrelation causes measured covariances smaller than would otherwise be expected, and in extreme cases may cause the selection of an erroneous time lag. Medium decorrelation limits the magnitude of the path separations that can be used (generally to less than 1 m for optical instruments), constrains

measurement precision, and creates ambiguity in crosswind measurements when winds are light and variable.

The principle of optical scintillometer operation can be illustrated with a simple eddy model presented by Clifford et al. (1974). Figure A-1 shows an optical path (SL), established between the transmitter and receiver, and a turbulent eddy of radius r at path position z. The turbulent eddy represents a density discontinuity moving across the optical path, and its index of refraction creates a new path SAL. This eddy is illuminated by a spherical wave of wavelength λ. The illuminated eddy produces a diffraction pattern observed at L, the size and contrast of which are determined by z, r, λ, and the refractive-index fluctuation ΔN of the eddy. Eddies at path position z which satisfy the condition SAL- SL = $\lambda/2$ produce strong scintillations at L through destructive interference. This condition is satisfied by a Fresnel-zone size eddy of radius

$$r = [\lambda z(1-z/L)]^{1/2} \qquad \text{(A-2)}$$

Eddies of radius larger or smaller than r have focal lengths shorter or longer than L and therefore contribute less to the variance in irradiance received at L. Sensitivities to the various portions of the optical path are defined by weighting functions. Weighting functions are determined by appropriate transmitter-receiver aperture designs.

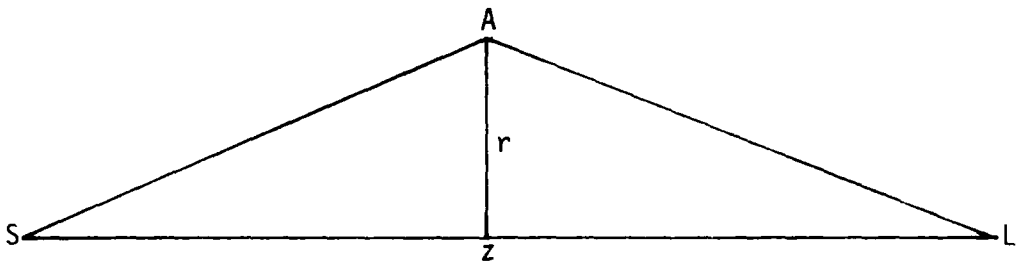

Figure A-1. The Geometry of a Simple Eddy Model Consisting of a Source S Illuminating an Eddy of Radius r at Position z Along the Optical Path. The Resultant Scintillations are Observed at Position L (After Clifford et al., 1974).

The variance in received irradiance is related to C_N^2 through the Tatarskii (1961) first order theory of scintillation. This theory is based on simple superposition of the effects of independent eddy encounters along the path. It predicts that, for a given path length L and free-space wavenumber k ($k=2\pi/\lambda$), the proportionality relationship between the log-amplitude variance in irradiance of the spherical wave (σ_t^2) and C_N^2 is

$$\sigma_t^2 = 0.124\ k^{7/6}\ L^{11/6}\ C_N^2 \qquad \text{(A-3)}$$

Equation (A-3) is valid for σ_t^2 less than 0.3. In stronger turbulence, the illuminating wavefront is no longer spherical due to distortion by previous eddies, and the proportionality between C_N^2 and σ_t^2 no longer remains constant. This condition, known as saturation, constrains the length of the optical path over which the scintillometer can be operated. Saturation and the signal-to-noise ratio, which decreases with path length, are the two major constraints on instrument range.

INTENTIONALLY BLANK

APPENDIX B: DESCRIPTION OF DPG SPECTRUM ANALYSIS PROGRAM

Spectrum analysis of time series data provides statistical measures of instrument performance and insight into the physics governing the interactions between sets of time series data. Simple linear correlation coefficients are not applicable to time series data because significance tests are based on the hypothesis that the variate samples are uncorrelated. Because significant autocorrelation often exists in time series data, this hypothesis is seriously violated. Also, the true relationship between two time series can be obscured by an in-phase relationship at some frequencies and an out-of-phase or phase-lagged relationship at other frequencies. A solution to some time series analysis problems lies in the multivariate analyses applied to spectra of time series. These analyses can be accomplished after a Fourier transformation of the series from the time domain to the frequency domain. Transformation partitions the power (energy expenditure per unit time) of the time series into harmonic frequency components. For winds, "power" is equivalent to variance per unit time. The total power of the process is equal to the sum of the contributions by the harmonic components. The advantage of power spectrum analysis over the usual multivariate analysis is that the amount of power contributed by one harmonic is independent of the amplitudes, phases, and frequencies of the other harmonics in the time series (Koopmans, 1974).

Relationships between two time series can be evaluated by examination of the spectra from the two series and their complex products, the cross spectrum, phase (PHASE), and coherence (COH). The cross spectrum is represented by the cospectrum (COS) and quadrature (QUAD). The cospectrum is analogous to an in-phase covariance between the two spectra, and the quadrature spectrum is a similar measure phase-shifted 1/4 wavelength (90°). COS and QUAD define the cross spectrum covariance components in a Cartesian-like coordinate system, while PHASE and COH express these components in a normalized polar coordinate system. PHASE, a representation of the angular relationship between two spectra, is defined as

$$\text{PHASE} = \text{ATAN2}(\text{QUAD}/\text{COS}), \tag{B-1}$$

where ATAN2 is defined in FORTRAN as the arctangent function expanded to the range $-\pi$ to π. PHASE is presented in degrees. COH, the squared coefficient of coherence, is a measure of the correlation between two time series as a function of frequency given by

$$\text{COH} = (\text{COS}^2 + \text{QUAD}^2) / (\text{SPCTR1}) * (\text{SPCTR2}), \tag{B-2}$$

where SPCTR1 and SPCTR2 are the spectral components of time series 1 and 2, respectively. COH is dimensionless and ranges in magnitude from 0 to 1. Statistical significance tests can be applied to coherence data as detailed in Koopmans (1974).

Fourier transformation in the DPG spectrum analysis program is achieved using a modification of the Fast Fourier Transform (FFT) procedures provided to DPG by the NOAA ERL/WPL, as described in Kaimal and Gaynor (1983). The spectra produced by this FFT are logarithmically smoothed and scaled to meter-kilogram-second (MKS) units by multiplying each harmonic component by its frequency. Table B.1 is a sample of spectra and their derived components. Spectral analysis techniques are discussed in detail by Koopmans (1974) and Jenkins and Watts (1968).

Table B.1. Spectra From Scintillometer Path Segments 1/5W and 1/5E.

SPECTRA DATA SUMMARY

SPECTRAL VALUES

Frequency HZ	Spectr1 (MKS**2)	Spectr2 (MKS**2)	COS (MKS**2)	QUAD (MKS**2)	PHASE Deg	COH
0.0006510	0.0149386	0.0161295	0.0154235	0.0017515	6.	1.000
0.0009766	0.0256345	0.0237723	0.0246550	-0.0012347	357.	1.000
0.0013021	0.0030787	0.0047646	0.0037214	-0.0009057	346.	1.000
0.0016276	0.1233213	0.1117816	0.1169572	0.0102984	5.	1.000
0.0021105	0.0309811	0.0321057	0.0313826	-0.0017177	357.	0.993
0.0027626	0.0040014	0.0063824	0.0048797	-0.0009015	350.	0.964
0.0035671	0.0685380	0.0560686	0.0618616	0.0002715	0.	0.996
0.0046964	0.0420406	0.0428175	0.0419824	0.0016084	2.	0.981
0.0062978	0.0685687	0.0585709	0.0630620	0.0021566	2.	0.991
0.0082623	0.0411610	0.0388346	0.0396976	-0.0008099	359.	0.986
0.0106653	0.0188904	0.0203057	0.0189336	-0.0003459	359.	0.935
0.0139046	0.0494865	0.0490781	0.0488862	-0.0009532	359.	0.984
0.0180887	0.0231475	0.0233634	0.0228077	-0.0004325	359.	0.962
0.0235842	0.0214758	0.0198889	0.0201379	-0.0003157	359.	0.950
0.0306794	0.0214200	0.0189295	0.0196526	0.0006133	2.	0.953
0.0398865	0.0155027	0.0146611	0.0145780	0.0000596	0.	0.935
0.0516774	0.0138524	0.0141710	0.0134470	-0.0005159	358.	0.922
0.0669952	0.0094777	0.0085844	0.0082342	0.0004016	3.	0.835
0.0868655	0.0066777	0.0075837	0.0065119	-0.0000856	359.	0.838
0.1126612	0.0044040	0.0044251	0.0036708	-0.0001420	358.	0.692
0.1462500	0.0032896	0.0035531	0.0025843	0.0001137	3.	0.573

APPENDIX C. GMQ-11 SITING AND PERFORMANCE CONSIDERATIONS

The aerovane is an extensively tested design (Mazzarella, 1954; Finkelstein, 1981) that has been used successfully over several decades for general wind measurements above the surface boundary layer. However, the size and inertia of the GMQ-11 aerovane could adversely affect its performance under some field conditions. Table C.1 lists the manufacturer's performance specifications for the Belfort Type L aerovane transmitter, a commercial equivalent of the GMQ-11.

Table C.1. Manufacturer's Performance Specifications for the Belfort Type L Aerovane Transmitter.

Specification	6-Blade Impeller	Vane Housing
Threshold (m/s)	0.8	2.2, 8° offset
Distance Constant (m)	4.6	10.4
Accuracy (%)	±1	±3
Damping Ratio	-----	0.3

Studies of rotating anemometer response in turbulent wind fields (MacCready, 1966; Acheson, 1970) report systematic overspeeding when mechanical wind sensors are used in turbulent wind fields, and a recent investigation by Mori and Mitsuta (1988) illustrates measurement problems common to aerovane-type instruments. Hyson (1972) shows that overspeeding occurs as a consequence of a second order velocity ratio term in the torque equation for rotating anemometers. This term causes rotating anemometers to gain energy faster than they shed energy, the net effect being a measured wind speed higher than the true wind speed. This effect increases as the ratio of anemometer response distance to dominant turbulence scales increases. Dominant turbulence scales become progressively smaller as surface roughness or proximity to the surface increases. Consequently, a GMQ-11 response distance of 4.6 m for the impeller and 10.4 m for the vane housing suggest that overspeeding could be a problem for a GMQ-11 mounted at 2 m, particularly when located downwind of a major roughness feature. Testing the GMQ-11 response to the turbulent wind field along the B-1 anemometer line was beyond the scope of this report, but the results of Acheson (1970) suggest an overspeed bias on the order of 5 to 10 percent for the GMQ-11s deployed along the B-1 anemometer line.

Another source of measurement error common to anemometer-vane systems occurs as a result of the separate averaging of wind-speed and wind-direction measurements when the requirement is a crosswind component of the wind vector. This is known as a data processing or DP error (MacCready, 1966). The error occurs when wind speeds and directions are averaged separately over a time interval to produce a "mean" wind speed and wind direction, as is done with GMQ-11 data. The wind speed DP error is zero if the wind direction is invariant in time, but with variable wind directions the net effect is an overestimate of the crosswind component. The DP error is usually on the order of 1 or 2 percent, but can be 5 percent or greater under highly variable wind conditions.

APPENDIX D: SONIC ANEMOMETER PERFORMANCE CONSIDERATIONS

The basic unit of measure for the sonic anemometer is time (t). The transmitter emits an ultrasonic adiabatic compression wave that propagates through the air at a velocity equal to the sum of the local speed of sound (c) plus the wind velocity component (v) along the transmitter-receiver axis. An inverse transit time solution for v, which eliminates c from the velocity solution, is given by

$$v = \frac{d}{2}\left[\frac{1}{t_1} - \frac{1}{t_2}\right] \qquad \text{(D-1)}$$

where t_1 is the compression wave travel time from transducer 1 to transducer 2, t_2 is the travel time in the opposite direction, and d is the acoustic path length. Measurement resolution is 0.01 m/s. Sonic anemometer performance is a function of clock time resolution, precision of the acoustic path length determination, and the instrument transfer function. Accuracy based on the resolution of time, atmospheric thermodynamics, and the electronic offset varies as a function of wind speed, but is typically ±0.05 m/s. This accuracy figure does not include transducer shadow effects on the transfer function. Further details of sonic anemometer performance are presented in Biltoft (1987).

Unlike the GMQ-11 aerovanes, sonic anemometers do not suffer delay distance effects or DP errors because they measure wind components without reacting mechanically to the wind field. The major source of error for sonic anemometers is transducer shadow effects. The transducer and supporting structures present an obstacle to the wind that deflects and retards flow across the acoustic path. Kaimal (1979) offers an algorithm to correct for transducer shadow effects as a function of transducer wind angle. A version of this algorithm has been incorporated into the data processing system of the ATI sonic anemometers used by DPG. However, the results from recent wind tunnel tests of the ATI sonic anemometer (Baker, 1988) show significant departures from the Kaimal algorithm and indicate a dependency on wind speed as well as transducer wind angle.

Shadowing effects were derived by Kaimal (1979) using low turbulence wind tunnels. A fully turbulent atmosphere should tend to dissipate shadowing effects more rapidly than the wind tunnel. Therefore, it is possible that an overcorrection is being applied in the fully turbulent atmosphere. This issue must be considered unresolved until data from the 1988 sonic anemometer intercomparison tests at the Boulder Atmospheric Observatory are analyzed. Until these transfer function uncertainties are resolved, mean wind measurements with the sonic anemometer along the B-1 line are expected to have an uncertainty on the order of 5 percent (B. Baker, personal communication), which includes a possible overspeeding bias due to overcompensation for shadowing effects.

Sonic anemometers are calibrated in a temperature-controlled zero wind chamber where the thermodynamic and electronic delay effects are defined. These effects are subsequently accounted for in the instrument's data transfer function. For instruments using the inverse time solution presented in Equation (D-1), temperature effects accounted for during calibration should not bias the data. A detailed discussion of sonic anemometer calibration is presented in Biltoft (1987).

APPENDIX E: REFERENCES

Acheson, D., 1970: Response of cup and propeller rotors and wind direction vanes to turbulent wind fields. Meteor. Monogr., 33, 252-261.

Baker, C.B., 1987: Experimental determination of transducer shadow effects on a sonic anemometer. U.S. Environmental Protection Agency (unpublished manuscript).

Biltoft, C.A., 1987: Development of sonic anemometer software. Report No. DPG-FR-88-702, U.S. Army Dugway Proving Ground, Dugway, UT.

Camp, D.W., and R.E. Turner, 1970: Response tests of cup, vane, and propeller wind sensors. J. Geophys. Res., 75, 5265-5270.

Clifford, S.F., G. Ochs, R. Lawrence, 1974: Saturation of optical scintillation by strong turbulence. J. Opt. Soc. Amer., 64, 148-154.

Finkelstein, P.L.,1981: Measuring the dynamic performance of wind vanes. J. Appl. Meteor., 20, 588-594.

Finkelstein, P., J.C. Kaimal, J. Gaynor, M. Graves, and T. Lockhart, 1986: Comparison of wind monitoring systems. Part I: In situ sensors. J. Atmos. Oceanic Tech., 3, 583-593.

Gill, G.C., 1973: The helicoid anemometer. Atmosphere, 11, 145-155.

Hoehne, W., 1971: Standardized functional tests. NOAA TM NWST&EL-12, U.S. Dept. of Commerce, Sterling VA.

Hyson, P., 1972: Cup anemometer response to fluctuating wind speeds. J. Appl. Meteor., 11, 843-848.

Jenkins, G.M., and D.G. Watts, 1968: Spectral Analysis and its Applications. Holden-Day, San Francisco, 525 pp.

Kaimal, J.C., 1979: Sonic anemometer measurement of atmospheric turbulence. Proc. Dynamic Flow Conference, Skovlunde, Denmark, DISA Electronic A/S, 551-565.

Kaimal, J.C., and J.E. Gaynor, 1983: The Boulder Atmospheric Observatory. J. Appl Meteor., 22, 863-880.

Koopmans, L., 1974: The Spectral Analysis of Time Series. The Academic Press, New York, 366 pp.

Lumley, J.L., and H.A. Panofsky, 1964: The Structure of Atmospheric Turbulence. Interscience-Wiley, 239 pp.

MacCready, P.B., 1966: Mean wind speed measurements in turbulence. J. Appl. Meteor., 5, 219-225.

Mazzarella, D.A., 1954: Wind tunnel tests on seven aerovanes. The Review of Scientific Instruments, 25, 63-68.

McCoy, R., 1976: The effect of wind on flat-fire trajectories. BRL Report No. 1900,(AD B012872L). U.S. Army Ballistic Research Laboratories, Aberdeen Proving Ground, MD.

Mori, Y., and Y. Mitsuta, 1988: Some problems in tower wind observations by the propeller-type anemometer. Symposium on Lower Tropospheric Profiling: Needs and Technologies, AMS, Boulder, CO (Also submitted for publication in special issue of J. Atmos. Oceanic Tech.).

Ochs, G.R., J.J. Wilson, R. George, and R. J. Lataitis, 1987: THP 025, Optical crosswind profiling system. J. Opt. Soc. Amer., Vol 13, 1-144.

Ochs, G.R., J.J. Wilson, S. Abbott, and R. George, 1988: Crosswind Profiler Model II. NOAA Technical Memorandum ERL/WPL 152.

Silverman, B, 1968: The effect of spatial averaging on spectrum estimation. J. Appl. Meteor., 7, 168-172.

Tatarskii, V.I., 1961: Wave Propagation in a Turbulent Medium. Dover, 285 pp.

Wyngaard, J.C., 1973: On Surface-Layer Turbulence. Workshop in Micrometeorology, D.A. Haugen, Ed., Amer. Meteor. Soc., Boston, 101-149.